Static quark-antiquark pairs at finite temperature

Nora Brambilla, Jacopo Ghiglieri, and Antonio Vairo
Dipartimento di Fisica dell'Università di Milano and INFN via Celoria 16, 20133 Milan, Italy

Péter Petreczky
RIKEN-BNL Research Center and Physics Department, Brookhaven National Laboratory, Upton, New York 11973, USA
(Received 9 April 2008; published 21 July 2008)

In a framework that makes close contact with modern effective field theories for nonrelativistic bound states at zero temperature, we study the real-time evolution of a static quark-antiquark pair in a medium of gluons and light quarks at finite temperature. For temperatures ranging from values larger to smaller than the inverse distance of the quark and antiquark, $1/r$, and at short distances, we derive the potential between the two static sources, and calculate their energy and thermal decay width. Two mechanisms contribute to the thermal decay width: the imaginary part of the gluon self-energy induced by the Landau damping phenomenon, and the quark-antiquark color-singlet to color-octet thermal breakup. Parametrically, the first mechanism dominates for temperatures such that the Debye mass is larger than the binding energy, while the latter, which we quantify here for the first time, dominates for temperatures such that the Debye mass is smaller than the binding energy. If the Debye mass is of the same order as $1/r$, our results are in agreement with a recent calculation of the static Wilson loop at finite temperature. For temperatures smaller than $1/r$, we find new contributions to the potential, both real and imaginary, which may be relevant to understand the onset of heavy quarkonium dissociation in a thermal medium.

DOI: 10.1103/PhysRevD.78.014017 PACS numbers: 12.38.−t, 12.38.Bx, 12.38.Mh, 12.39.Hg

I. INTRODUCTION

The study of heavy quark-antiquark pairs in a thermal medium at temperature T has received a lot of attention since it was suggested that quarkonium dissociation due to color screening may be a striking signature of the quark-gluon plasma formation [1]. Based on this idea and the assumption that medium effects can be understood in terms of a temperature-dependent potential, the problem of quarkonium dissociation has been addressed in terms of potential models with screened temperature-dependent potentials over the past 20 years (see, e.g., Refs. [2–4] for some representative works). A derivation from QCD of the in-medium quarkonium potential has not appeared in the literature so far and expectedly not all medium effects can be incorporated into a potential. A first step toward a QCD derivation of the quarkonium potential at finite temperature has been a recent calculation [5] of the static Wilson loop in the imaginary-time formalism at order α_s. After analytical continuation to real time, the calculation shows a real part, which is a screened Coulomb potential, and an imaginary part that may be traced back to the scattering of particles in the medium carrying momenta of order T with spacelike gluons, a phenomenon also known as Landau damping. Some applications can be found in [6,7]. First principle calculations of quarkonium properties at finite temperature include calculations of Euclidean correlation functions in lattice QCD and the reconstruction of the corresponding spectral functions using the maximum entropy method. At the present, however, a reliable determination of the quarkonium spectral functions from the lattice data appears very difficult due to statistical errors and lattice discretization effects (see the discussion in Ref. [8] and references therein).

In this work, we will study static quark-antiquark pairs in a thermal bath in real-time formalism (see, e.g., [9]) and in a framework that makes close contact with effective field theories (EFTs) for nonrelativistic bound states at $T = 0$ [10]. In this framework, we will address the problem of defining and deriving the potential between the two static sources, and we will calculate their energy and thermal decay width. We will describe the system for temperatures that range from larger to smaller values with respect to the inverse distance of the quark and antiquark, $1/r$. In some range, we will agree with previous findings; for temperatures lower than the inverse distance of the quark and antiquark, we will find new contributions to the potential, both real and imaginary, with a nontrivial analytical structure. In particular, we will point out the existence of a new type of process that contributes to the quark-antiquark thermal decay width besides the Landau damping.

We will deal with static quarks only. The static case is relevant also for the study of bound states made of quarks with a large but finite mass m, like quarkonia, in a thermal medium. Quarkonium is expected to exist in the medium if the temperature and the other thermodynamical scales are much lower than m. In this situation, one may consistently integrate out the mass from QCD and expand order by order in $1/m$. The leading order of the expansion corresponds to QCD with a static quark and a static antiquark. Higher-order corrections in $1/m$ may be systematically

included in the framework of nonrelativistic QCD (NRQCD) [11].

Bound states at finite temperature are systems characterized by many energy scales. There are the thermodynamical scales that describe the motion of the particles in the thermal bath: the temperature scale T (we will not distinguish between T and multiple of πT), the Debye mass m_D, which is the scale of the screening of the chromoelectric interactions, and lower energy scales. In the weak-coupling regime, which we will assume throughout this work, one has $m_D \sim gT \ll T$. Moreover, there are the scales typical of the bound state. In the case of a system of two static sources, the scales may be identified with the inverse of the quark-antiquark distance r and the static potential, the first being much larger than the second. We will also assume that both scales are much larger than the typical hadronic scale $\Lambda_{\rm QCD}$, i.e., we will concentrate on the short-distance part of the potential (explicit expressions of the potential, whose derivation is the main scope of the paper, can be found in the following sections; for the purpose of the power counting the leading term is sufficient). This may be the part of the potential relevant for the lowest quarkonium resonances like the J/ψ or the $\Upsilon(1S)$, which are the most tightly bound states. Thermodynamical and bound-state scales get entangled and different hierarchies are possible. Bound states are expected to dissolve in the bath at temperatures such that m_D is larger than the typical inverse size of the bound state. Hence we will concentrate on the situation $1/r \gtrsim m_D$ (i.e., $1/r \gg m_D$ or $1/r \sim m_D$), and distinguish between the two cases $1/r \gg T$ and $1/r \ll T$.

The paper is organized as follows. Sections II and III are introductory: they deal with QCD with static sources, which we call static QCD for short, but do not include bound states. In Sec. II, we write the quark and gluon propagators in static QCD at finite T. In Sec. III, we summarize one-loop finite T contributions in static QCD that are relevant to the present work. In Sec. IV, we introduce the relevant EFTs and calculate the static potential in a situation where the inverse distance between the static quark and antiquark is larger than the temperature of the thermal bath: $1/r \gg T \gg m_D$. When T is as small as the binding energy, we also calculate the leading thermal contribution to the static energy and the decay width. In Sec. V, we provide an alternative derivation of the potential in perturbative QCD. In Sec. VI, we calculate the static potential in the situation $T \gg 1/r \gtrsim m_D$. In Sec. VII, we summarize and discuss our results and list some possible developments.

II. STATIC QCD AT FINITE T

We consider here QCD with a static quark and antiquark; in particular, we write the quark, antiquark, and the gluon propagators at finite T. To simplify the notation, we will drop the color indices from the propagators. Throughout the paper, the complex time contour for the evaluation of the real-time thermal expectation values goes from a real initial time $t_{\rm i}$ to a real final time $t_{\rm f}$, from $t_{\rm f}$ to $t_{\rm f} - i0^+$, from $t_{\rm f} - i0^+$ to $t_{\rm i} - i0^+$, and from $t_{\rm i} - i0^+$ to $t_{\rm i} - i/T$. The propagators will be given with this conventional choice of contour. Furthermore, the following notations will be used. We indicate thermal averages as

$$\langle O \rangle_T = \frac{{\rm Tr}\{e^{-H/T} O\}}{{\rm Tr}\{e^{-H/T}\}}, \tag{1}$$

where H is the Hamiltonian of the system. We also define

$$n_{\rm F}(k^0) = \frac{1}{e^{k^0/T} + 1}, \tag{2}$$

$$n_{\rm B}(k^0) = \frac{1}{e^{k^0/T} - 1}. \tag{3}$$

A. Quark propagator

In order to show the behavior of static sources in a thermal bath, it may be useful to consider first a quark (or antiquark) with a large but finite mass m, $m \gg T$, and then perform the $m \to \infty$ limit.

We define the propagators

$$S^{>}_{\alpha\beta}(x) = \langle \psi_\alpha(x) \psi^\dagger_\beta(0) \rangle_T, \tag{4}$$

$$S^{<}_{\alpha\beta}(x) = -\langle \psi^\dagger_\beta(0) \psi_\alpha(x) \rangle_T, \tag{5}$$

where ψ is the Pauli spinor field that annihilates the fermion (in the following, the Pauli spinor field that creates the antifermion will be denoted χ). The free propagators,

$$S^{>(0)}_{\alpha\beta} = \delta_{\alpha\beta} S^{>(0)}, \qquad S^{<(0)}_{\alpha\beta} = \delta_{\alpha\beta} S^{<(0)}, \tag{6}$$

satisfy the equations [in momentum space: $S(k) = \int d^4x e^{ikx} S(x)$]:

$$k^0 S^{>(0)}(k) = m S^{>(0)}(k), \tag{7}$$

$$k^0 S^{<(0)}(k) = m S^{<(0)}(k), \tag{8}$$

where we have neglected corrections of order $1/m$ or smaller: they will eventually vanish in the $m \to \infty$ limit.

If the heavy quarks are part of the thermal bath, they satisfy the Kubo-Martin-Schwinger relation:

$$S^{<(0)}(k) = -e^{-k^0/T} S^{>(0)}(k). \tag{9}$$

From the equal-time canonical commutation relation it follows the sum rule

$$\int \frac{dk^0}{2\pi} (S^{>(0)}(k) - S^{<(0)}(k)) = 1. \tag{10}$$

The solutions of the Eqs. (7)–(10) are

$$S^{>(0)}(k) = (1 - n_{\rm F}(k^0)) 2\pi \delta(k^0 - m), \tag{11}$$

$$S^{<(0)}(k) = -n_{\rm F}(k^0)2\pi\delta(k^0 - m). \tag{12}$$

The spectral density $\rho_{\rm F}^{(0)}$ is given by

$$\rho_{\rm F}^{(0)}(k) = S^{>(0)}(k) - S^{<(0)}(k) = 2\pi\delta(k^0 - m), \tag{13}$$

and the free propagator,

$$S^{(0)}(x) = \theta(x^0)S^{>(0)}(x) - \theta(-x^0)S^{<(0)}(x), \tag{14}$$

is given in momentum space by

$$S^{(0)}(k) = \frac{i}{k^0 - m + i\epsilon} - n_{\rm F}(k^0)2\pi\delta(k^0 - m). \tag{15}$$

In the static limit $m \to \infty$, the propagators simplify because $n_{\rm F}(m) \to 0$ for $m \to \infty$. Moreover, we may get rid of the explicit mass dependence by means of the field redefinition $\psi \to \psi e^{-imt}$, which amounts to change $k^0 - m$ to k^0 in the expressions for the propagators and the spectral density; they read now

$$S^{>(0)}(k) = 2\pi\delta(k^0), \tag{16}$$

$$S^{<(0)}(k) = 0, \tag{17}$$

$$S^{(0)}(k) = \frac{i}{k^0 + i\epsilon}, \tag{18}$$

$$\rho_{\rm F}^{(0)}(k) = 2\pi\delta(k^0). \tag{19}$$

The free static propagator is the same as at zero temperature. On the other hand, if we would have assumed from the beginning that $S^{<(0)}(k) = 0$, i.e., that there is no backward propagation of a static quark (in agreement with the Kubo-Martin-Schwinger formula in the $m \to \infty$ limit) then, together with the equations of motion $k^0 S^{>(0)}(k) = 0$, $k^0 S^{<(0)}(k) = 0$ (obtained after removing m via field redefinitions) and the sum rule (10), we would have obtained Eqs. (16), (18), and (19).

The real-time free static propagator for the quark reads

$$\begin{aligned}\mathbf{S}^{(0)}_{\alpha\beta}(k) &= \delta_{\alpha\beta}\begin{pmatrix} S^{(0)}(k) & S^{<(0)}(k) \\ S^{>(0)}(k) & (S^{(0)}(k))^* \end{pmatrix} \\ &= \delta_{\alpha\beta}\begin{pmatrix} \frac{i}{k^0+i\epsilon} & 0 \\ 2\pi\delta(k^0) & \frac{-i}{k^0-i\epsilon} \end{pmatrix},\end{aligned} \tag{20}$$

and for the antiquark

$$\mathbf{S}^{(0)}_{\alpha\beta}(k) = \delta_{\alpha\beta}\begin{pmatrix} \frac{i}{-k^0+i\epsilon} & 0 \\ 2\pi\delta(k^0) & \frac{-i}{-k^0-i\epsilon} \end{pmatrix}. \tag{21}$$

The main observation here is that, since the $[\mathbf{S}^{(0)}_{\alpha\beta}(k)]_{12}$ component vanishes, the static quark (antiquark) fields labeled 2 never enter in any physical amplitude, i.e., any amplitude that has the physical fields, labeled 1, as initial and final states. Hence, when considering physical amplitudes, the static fields 2 decouple and may be ignored.

The propagator $\mathbf{S}^{(0)}_{\alpha\beta}$ may be written in a diagonal form as

$$\mathbf{S}^{(0)}_{\alpha\beta}(k) = \mathbf{U}^{(0)}\begin{pmatrix} \frac{i}{k^0+i\epsilon} & 0 \\ 0 & \frac{-i}{k^0-i\epsilon} \end{pmatrix}\mathbf{U}^{(0)}, \tag{22}$$

where

$$\begin{aligned}\mathbf{U}^{(0)} &= \begin{pmatrix} 1 & 0 \\ 1 & 1 \end{pmatrix}, \quad \text{and for further use} \\ [\mathbf{U}^{(0)}]^{-1} &= \begin{pmatrix} 1 & 0 \\ -1 & 1 \end{pmatrix}.\end{aligned} \tag{23}$$

Throughout the paper, we will use bold-face letters to indicate 2×2 matrices in the real-time formalism.

B. Gluon propagator

The gluon propagator in the real-time formalism can be written as [9]

$$\mathbf{D}_{\alpha\beta}(k) = \begin{pmatrix} D_{\alpha\beta}(k) & D^{<}_{\alpha\beta}(k) \\ D^{>}_{\alpha\beta}(k) & (D_{\alpha\beta}(k))^* \end{pmatrix}, \tag{24}$$

where

$$D^{>}_{\alpha\beta}(k) = \int d^4x e^{ik\cdot x}\langle A_\alpha(x)A_\beta(0)\rangle_T, \tag{25}$$

$$D^{<}_{\alpha\beta}(k) = \int d^4x e^{ik\cdot x}\langle A_\beta(0)A_\alpha(x)\rangle_T, \tag{26}$$

$$\begin{aligned}D_{\alpha\beta}(k) = \int d^4x e^{ik\cdot x}[&\theta(x_0)\langle A_\alpha(x)A_\beta(0)\rangle_T \\ &+ \theta(-x_0)\langle A_\beta(0)A_\alpha(x)\rangle_T].\end{aligned} \tag{27}$$

Gluons being bosonic fields, the Kubo-Martin-Schwinger relation reads

$$D^{<}(k) = e^{-k^0/T}D^{>}(k), \tag{28}$$

from which it follows that

$$D^{>}_{\alpha\beta}(k) = (1 + n_{\rm B}(k^0))\rho_{{\rm B}\alpha\beta}(k), \tag{29}$$

$$D^{<}_{\alpha\beta}(k) = n_{\rm B}(k^0)\rho_{{\rm B}\alpha\beta}(k), \tag{30}$$

where

$$\rho_{{\rm B}\alpha\beta}(k) = D^{>}_{\alpha\beta}(k) - D^{<}_{\alpha\beta}(k), \tag{31}$$

is the spectral density.

We may express $\mathbf{D}_{\alpha\beta}$ also in terms of the retarded and advanced propagators $D^{\rm R}_{\alpha\beta}$ and $D^{\rm A}_{\alpha\beta}$:

$$D^{\rm R}_{\alpha\beta}(k) = \int d^4x e^{ik\cdot x}\theta(x_0)\langle[A_\alpha(x), A_\beta(0)]\rangle_T, \tag{32}$$

$$D^{\rm A}_{\alpha\beta}(k) = -\int d^4x e^{ik\cdot x}\theta(-x_0)\langle[A_\alpha(x), A_\beta(0)]\rangle_T; \tag{33}$$

we have

$$\rho_{\mathrm{B}\alpha\beta}(k) = D^{\mathrm{R}}_{\alpha\beta}(k) - D^{\mathrm{A}}_{\alpha\beta}(k), \tag{34}$$

$$D_{\alpha\beta}(k) = D^{\mathrm{R}}_{\alpha\beta}(k) + D^{<}_{\alpha\beta}(k) = D^{\mathrm{A}}_{\alpha\beta}(k) + D^{>}_{\alpha\beta}(k) = \frac{D^{\mathrm{R}}_{\alpha\beta}(k) + D^{\mathrm{A}}_{\alpha\beta}(k)}{2} + \left(\frac{1}{2} + n_{\mathrm{B}}(k^0)\right)\rho_{\mathrm{B}\alpha\beta}(k). \tag{35}$$

In the free case, in Coulomb gauge, the longitudinal and transverse propagators have the following expressions [12]:

$$\mathbf{D}^{(0)}_{00}(\vec{k}) = \begin{pmatrix} \frac{i}{\vec{k}^2} & 0 \\ 0 & -\frac{i}{\vec{k}^2} \end{pmatrix}, \tag{36}$$

$$\mathbf{D}^{(0)}_{ij}(k) = \left(\delta_{ij} - \frac{k^i k^j}{\vec{k}^2}\right) \times \left\{ \begin{pmatrix} \frac{i}{k^2+i\epsilon} & \theta(-k^0)2\pi\delta(k^2) \\ \theta(k^0)2\pi\delta(k^2) & -\frac{i}{k^2-i\epsilon} \end{pmatrix} + 2\pi\delta(k^2) n_{\mathrm{B}}(|k^0|) \begin{pmatrix} 1 & 1 \\ 1 & 1 \end{pmatrix} \right\}, \tag{37}$$

where $k^2 = (k^0)^2 - \vec{k}^2$. Note that the longitudinal part of the gluon propagator in Coulomb gauge does not depend on the temperature. The temperature enters only the transverse part, which splits in the sum of a $T = 0$ piece and a thermal one.

C. Lagrangian

The Lagrangian of QCD with a static quark, a static antiquark, and n_f massless quark fields q_i is

$$\mathcal{L} = -\frac{1}{4} F^a_{\mu\nu} F^{a\mu\nu} + \sum_{i=1}^{n_f} \bar{q}_i i \not{D} q_i + \psi^\dagger i D_0 \psi + \chi^\dagger i D_0 \chi, \tag{38}$$

where $iD^0 = i\partial_0 - gA^0$, $i\vec{D} = i\vec{\nabla} + g\vec{A}$, and $igF_{\mu\nu} = [D_\mu, D_\nu]$. The free static quark propagator is given by Eq. (20), the free static antiquark propagator by Eq. (21), and the free gluon propagator (in Coulomb gauge) by Eqs. (36) and (37). Note that transverse gluons do not couple directly to static quarks.

III. ONE-LOOP FINITE T CONTRIBUTIONS IN STATIC QCD

Throughout this work, we will assume that T, $gT \gg \Lambda_{\mathrm{QCD}}$; this enables us to evaluate thermal properties of QCD in the weak-coupling regime. In this section, we consider one-loop thermal contributions to the static quark propagator, quark-gluon vertices, and gluon propagator. When the loop momenta and energies are taken at the scale T and the external momenta are much lower, so that we may expand with respect to them, these correspond to the hard thermal loop (HTL) contributions [13].

The one-loop contributions to the static quark self-energy, to the static quark longitudinal-gluon vertex and to the static quark transverse-gluon vertex are displayed in Figs. 1–3, respectively. It is convenient to fix the Coulomb gauge. In that gauge, longitudinal gluons do not depend on the temperature [see Eq. (36)] and the above diagrams do not give thermal contributions. Moreover, if evaluated in dimensional regularization they vanish after expanding in the external momenta. Throughout this work, we will adopt the Coulomb gauge unless stated otherwise.

Momenta and energies of order T contribute to the gluon self-energy diagrams. Since only longitudinal gluons couple to static quarks, we will focus on the longitudinal part of the polarization tensor. This will be the only component of the gluon polarization tensor relevant to the paper. Diagrams contributing to the thermal part of the longitudinal-gluon polarization tensor in real-time formalism at one-loop order are shown in Fig. 4. In Sec. III A, we will give a general expression, and in Secs. III B, III C, and III D, we will expand it in some relevant limits.

FIG. 1. Self-energy diagram. The continuous line stands for a static quark, the dashed one for a longitudinal gluon.

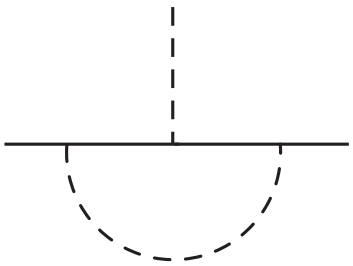

FIG. 2. Vertex correction to the static quark line; the incoming gluon is longitudinal.

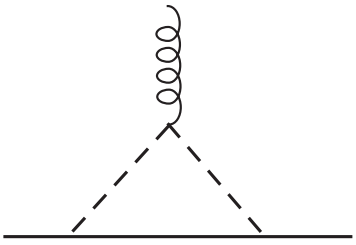

FIG. 3. Vertex correction to the static quark line; the incoming gluon is transverse.

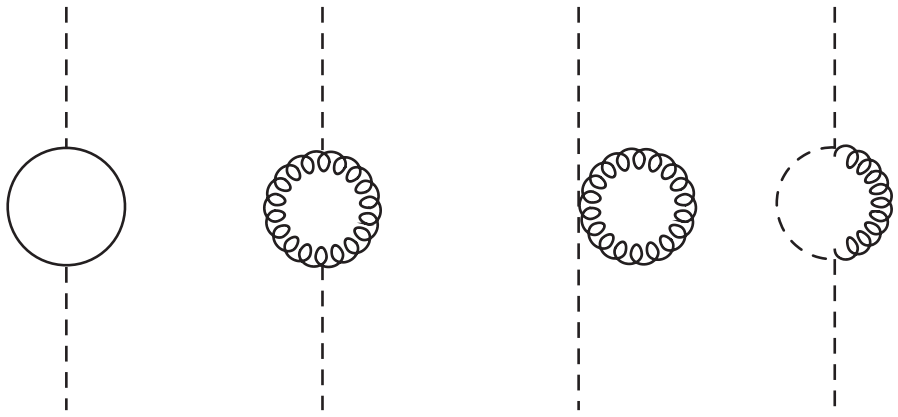

FIG. 4. Diagrams contributing to the longitudinal component of the gluon polarization tensor at one-loop order. The continuous loop stands for light (massless) quark loops, dashed lines for longitudinal gluons, and curly lines for transverse gluons. Ghosts do not contribute to the thermal part of the gluon polarization tensor [12].

A. The longitudinal-gluon polarization tensor

Summing up all thermal contributions from the diagrams of Fig. 4, we obtain (for details see [14])

$$[\Pi^{\mathrm{R}}_{00}(k)]_{\mathrm{thermal}} = [\Pi_{00}(k^0 + i\epsilon, \vec{k})]_{\mathrm{thermal}}, \tag{39}$$

$$[\Pi^{\mathrm{A}}_{00}(k)]_{\mathrm{thermal}} = [\Pi_{00}(k^0 - i\epsilon, \vec{k})]_{\mathrm{thermal}}, \tag{40}$$

$$[\Pi_{00}(k)]_{\mathrm{thermal}} = [\Pi_{00,\mathrm{F}}(k)]_{\mathrm{thermal}} + [\Pi_{00,\mathrm{G}}(k)]_{\mathrm{thermal}}, \tag{41}$$

$$\begin{aligned}[\Pi_{00,\mathrm{F}}(k)]_{\mathrm{thermal}} = \frac{g^2 T_F n_f}{2\pi^2} \int_{-\infty}^{+\infty} dq^0 |q^0| n_{\mathrm{F}}(|q^0|) \Bigg[2 - \left(\frac{4(q^0)^2 + k^2 - 4q^0 k^0}{4|q^0||\vec{k}|} \right) \ln \frac{k^2 - 2q^0 k^0 + 2|q^0||\vec{k}|}{k^2 - 2q^0 k^0 - 2|q^0||\vec{k}|} \\ + \left(\frac{4(q^0)^2 + k^2 + 4q^0 k^0}{4|q^0||\vec{k}|} \right) \ln \frac{k^2 + 2q^0 k^0 - 2|q^0||\vec{k}|}{k^2 + 2q^0 k^0 + 2|q^0||\vec{k}|} \Bigg],\end{aligned} \tag{42}$$

$$\begin{aligned}[\Pi_{00,\mathrm{G}}(k)]_{\mathrm{thermal}} = \frac{g^2 N_c}{2\pi^2} \int_{-\infty}^{+\infty} dq^0 |q^0| n_{\mathrm{B}}(|q^0|) \Bigg\{ 1 + \frac{(2q^0 - k^0)^2}{8(q^0)^2} - \frac{1}{2} - \frac{|\vec{k}|^2}{2(q^0)^2} + 2 \Bigg[\frac{|\vec{k}|}{2|q^0|} - \frac{(|\vec{k}|^2 + (q^0)^2)^2}{8|q^0|^3 |\vec{k}|} - \frac{(2q^0 - k^0)^2}{4(q^0 - k^0)^2} \\ \times \left(- \frac{(|\vec{k}|^2 + (q^0)^2)^2}{8|q^0|^3 |\vec{k}|} + \frac{|\vec{k}|}{2|q^0|} \right) \Bigg] \ln \left| \frac{|\vec{k}| - |q^0|}{|\vec{k}| + |q^0|} \right| \\ - \frac{(2q^0 - k^0)^2}{4} \Bigg[\frac{1}{2|q^0|\,|\vec{k}|} + \frac{1}{(q^0 - k^0)^2} \left(\frac{(k^2 - 2q^0 k^0)^2}{8|q^0|^3 |\vec{k}|} + \frac{k^2 - 2q^0 k^0}{2|q^0|\,|\vec{k}|} + \frac{|q^0|}{2|\vec{k}|} \right) \Bigg] \\ \times \ln \frac{k^2 - 2q^0 k^0 + 2|q^0|\,|\vec{k}|}{k^2 - 2q^0 k^0 - 2|q^0|\,|\vec{k}|} \Bigg\},\end{aligned} \tag{43}$$

where R stands for retarded, A for advanced, F labels the contribution coming from the loops of n_f massless quarks (first diagram of Fig. 4), and G labels the contribution from the second, third, and fourth diagram of Fig. 4. $N_c = 3$ is the number of colors and $T_F = 1/2$. In the context of the imaginary-time formalism, Eqs. (42) and (43) can be found also in textbooks such as [15]. The original derivation of (43) is in [16].

The retarded and advanced gluon self-energies contribute to the retarded and advanced gluon propagators. From the retarded and advanced gluon propagators we may derive the full propagator, the spectral density, and finally

all components of the 2×2 matrix of the real-time gluon propagator along the lines of Sec. II B. In the following, we study Eqs. (39)–(43) in different kinematical limits.

B. The longitudinal-gluon polarization tensor for $k^0 \ll T \sim |\vec{k}|$

The typical loop momentum q^0 is of order T. If we expand $[\Pi^{\mathrm{R}}_{00}(k)]_{\mathrm{thermal}}$ and $[\Pi^{\mathrm{A}}_{00}(k)]_{\mathrm{thermal}}$ in $k^0 \ll T \sim |\vec{k}|$ and keep terms up to order k^0, the result is

$$\begin{aligned}\mathrm{Re}[\Pi^{\mathrm{R}}_{00}(k)]_{\mathrm{thermal}} &= \mathrm{Re}[\Pi^{\mathrm{A}}_{00}(k)]_{\mathrm{thermal}} \\ &= \frac{g^2 T_F n_f}{\pi^2}\int_0^{+\infty} dq^0 q^0 n_{\mathrm{F}}(q^0)\left[2 + \left(\frac{|\vec{k}|}{2q^0} - 2\frac{q^0}{|\vec{k}|}\right)\ln\left|\frac{|\vec{k}| - 2q^0}{|\vec{k}| + 2q^0}\right|\right] \\ &\quad + \frac{g^2 N_c}{\pi^2}\int_0^{+\infty} dq^0 q^0 n_{\mathrm{B}}(q^0)\left[1 - \frac{\vec{k}^2}{2(q^0)^2} + \left(-\frac{q^0}{|\vec{k}|} + \frac{|\vec{k}|}{2q^0} - \frac{|\vec{k}|^3}{8(q^0)^3}\right)\ln\left|\frac{|\vec{k}| - 2q^0}{|\vec{k}| + 2q^0}\right|\right], \end{aligned} \tag{44}$$

$$\begin{aligned}\mathrm{Im}\,[\Pi^{\mathrm{R}}_{00}(k)]_{\mathrm{thermal}} &= -\mathrm{Im}[\Pi^{\mathrm{A}}_{00}(k)]_{\mathrm{thermal}} \\ &= \frac{2g^2 T_F n_f}{\pi}\frac{k^0}{|\vec{k}|}\int_{|\vec{k}|/2}^{+\infty} dq^0 q^0 n_{\mathrm{F}}(q^0) + \frac{g^2 N_c}{\pi}\frac{k^0}{|\vec{k}|}\left[\frac{\vec{k}^2}{8} n_{\mathrm{B}}(|\vec{k}|/2) + \int_{|\vec{k}|/2}^{+\infty} dq^0 q^0 n_{\mathrm{B}}(q^0)\left(1 - \frac{\vec{k}^4}{8(q^0)^4}\right)\right]. \end{aligned} \tag{45}$$

Equation (45) and the gluonic part of (44) are in agreement with [16].

C. The longitudinal-gluon polarization tensor for $k^0 \sim |\vec{k}| \ll T$

If we assume that all components of the external four-momentum are much smaller than the loop momentum $q^0 \sim T$, then we may expand $[\Pi^{\mathrm{R}}_{00}(k)]_{\mathrm{thermal}}$ and $[\Pi^{\mathrm{A}}_{00}(k)]_{\mathrm{thermal}}$ in $k^0 \sim |\vec{k}| \ll T$. At leading order, we obtain the well-known HTL expression for the longitudinal-gluon polarization tensor, which may be found, for instance, in [9]

$$\begin{aligned}\mathrm{Re}\,[\Pi^{\mathrm{R}}_{00}(k)]_{\mathrm{thermal}} &= \mathrm{Re}[\Pi^{\mathrm{A}}_{00}(k)]_{\mathrm{thermal}} \\ &= m_D^2\left(1 - \frac{k^0}{2|\vec{k}|}\ln\left|\frac{k^0 + |\vec{k}|}{k^0 - |\vec{k}|}\right|\right), \end{aligned} \tag{46}$$

$$\begin{aligned}\mathrm{Im}\,[\Pi^{\mathrm{R}}_{00}(k)]_{\mathrm{thermal}} &= -\mathrm{Im}[\Pi^{\mathrm{A}}_{00}(k)]_{\mathrm{thermal}} \\ &= m_D^2\frac{k^0}{|\vec{k}|}\frac{\pi}{2}\theta(-k^2), \end{aligned} \tag{47}$$

where m_D is the Debye mass:

$$m_D^2 = \frac{g^2 T^2}{3}(N_c + T_F n_f). \tag{48}$$

We have used that $\int_0^\infty dq^0 q^0 n_{\mathrm{F}}(q^0) = \pi^2 T^2/12$ and $\int_0^\infty dq^0 q^0 n_{\mathrm{B}}(q^0) = \pi^2 T^2/6$. Note that the expansions for $|\vec{k}| \to 0$ of (44) and (45) and those for $k^0 \to 0$ of (46) and (47) agree with each other at leading order.

1. The resummed longitudinal-gluon propagator

The longitudinal polarization tensor induces corrections to the longitudinal-gluon propagator:

$$D^{\mathrm{R,A}}_{00}(k) = \frac{i}{\vec{k}^2} - \frac{i}{\vec{k}^4}\Pi^{\mathrm{R,A}}_{00}(k) + \cdots. \tag{49}$$

Since $\Pi^{\mathrm{R,A}}_{00}$ contains a real and an imaginary part, also $D^{\mathrm{R,A}}_{00}$ acquires a real and an imaginary part.

If the typical momentum transfer is of the order of the Debye mass, $|\vec{k}| \sim m_D$, then the series in (49) needs to be resummed:

$$D^{\mathrm{R,A}}_{00}(k) = \frac{i}{\vec{k}^2 + \Pi^{\mathrm{R,A}}_{00}(k)}. \tag{50}$$

The resummed longitudinal propagator depends on k^0 and has a real and an imaginary part. The Debye mass m_D plays the role of a screening mass for longitudinal gluons whose momenta are such that $k^0 \ll T$ and $|\vec{k}| \sim m_D$. A study of the resummed gluon propagator in the real-time formalism may be found in [17].

The role of the screening mass can be made more evident if we assume further that $k^0 \ll |\vec{k}| \sim m_D \ll T$ and expand Eq. (50) in k^0 up to order k^0; then we obtain

$$D^{\mathrm{R,A}}_{00}(k) = \frac{i}{\vec{k}^2 + m_D^2} \pm \frac{\pi}{2}\frac{k^0}{|\vec{k}|}\frac{m_D^2}{(\vec{k}^2 + m_D^2)^2}, \tag{51}$$

where the $+$ and $-$ signs refer to the retarded and advanced propagators, respectively. The corresponding spectral density is

$$\rho_{\mathrm{B}00}(k) = D^{\mathrm{R}}_{00}(k) - D^{\mathrm{A}}_{00}(k) = \pi \frac{k^0}{|\vec{k}|} \frac{m_D^2}{(\vec{k}^2 + m_D^2)^2}. \quad (52)$$

Following Sec. II B and expanding in k^0 also the Bose factor, $n_{\mathrm{B}}(k^0) \approx T/k^0$, at leading order in k^0, we obtain that the resummed HTL longitudinal propagator in the real-time formalism is

$$\mathbf{D}_{00}(0,\vec{k}) = \frac{i}{\vec{k}^2 + m_D^2} \begin{pmatrix} 1 & 0 \\ 0 & -1 \end{pmatrix} + \pi \frac{T}{|\vec{k}|} \frac{m_D^2}{(\vec{k}^2 + m_D^2)^2} \begin{pmatrix} 1 & 1 \\ 1 & 1 \end{pmatrix}. \quad (53)$$

D. The longitudinal-gluon polarization tensor for $|\vec{k}| \gg T \gg k^0$

If we assume that $|\vec{k}| \gg T \gg k^0$, then the expression for the longitudinal-gluon polarization tensor may be extracted from Eqs. (44) and (45) by expanding for large $|\vec{k}|/T$. At leading order, we obtain

$$[\Pi^{\mathrm{R}}_{00}(k)]_{\mathrm{thermal}} = [\Pi^{\mathrm{A}}_{00}(k)]_{\mathrm{thermal}} = -\frac{N_c g^2 T^2}{18}. \quad (54)$$

The result is real and does not depend on k. Moreover, only the gluonic part of the polarization tensor contributes in this limit and at this order. Higher-order real corrections are suppressed by $T^2/\vec{k}^2$, while higher-order imaginary corrections are exponentially suppressed.

IV. BOUND STATES FOR $1/r \gg T$

Starting with this section, we shall address bound states made of a static quark and antiquark in QCD at finite T. Bound states introduce extra scales in the dynamics, besides T and m_D, that we have to account for. The most relevant one is the distance r between the quark and the antiquark. Throughout the paper, we will assume that $1/r \gg \Lambda_{\mathrm{QCD}}$. We will further assume that also the binding energy of the quark-antiquark static pair is larger than Λ_{QCD}.

First, we deal with the situation where the inverse distance of the two static sources is much larger than the temperature: $1/r \gg T$. Under this condition, we may integrate out $1/r$ from static QCD at $T = 0$ order by order in α_{s}. The EFT that we obtain is potential nonrelativistic QCD (pNRQCD) in the static limit [18,19], whose Lagrangian can be written as

$$\mathcal{L} = -\frac{1}{4} F^a_{\mu\nu} F^{a\mu\nu} + \sum_{i=1}^{n_f} \bar{q}_i i \not{D} q_i + \int d^3 r \, \mathrm{Tr}\left\{ \mathrm{S}^\dagger \left[i\partial_0 + C_F \frac{\alpha_{V_s}}{r} \right] \mathrm{S} + \mathrm{O}^\dagger \left[iD_0 - \frac{1}{2N_c} \frac{\alpha_{V_o}}{r} \right] \mathrm{O} \right\}$$
$$+ V_A \, \mathrm{Tr}\{\mathrm{O}^\dagger \vec{r} \cdot g\vec{E} \mathrm{S} + \mathrm{S}^\dagger \vec{r} \cdot g\vec{E} \mathrm{O}\} + \frac{V_B}{2} \mathrm{Tr}\{\mathrm{O}^\dagger \vec{r} \cdot g\vec{E} \mathrm{O} + \mathrm{O}^\dagger \mathrm{O} \vec{r} \cdot g\vec{E}\} + \cdots. \quad (55)$$

The fields $\mathrm{S} = S\mathbf{1}_c/\sqrt{N_c}$ and $\mathrm{O} = O^a T^a/\sqrt{T_F}$ are static quark-antiquark singlet and octet fields, respectively, $\vec{E}$ is the chromoelectric field: $E^i = F^{i0}$, and $C_F = (N_c^2 - 1)/(2N_c) = 4/3$. The trace is over the color indices. The matching coefficients α_{V_s}, α_{V_o}, V_A, V_B are at leading order: $\alpha_{V_s} = \alpha_{\mathrm{s}}$, $\alpha_{V_o} = \alpha_{\mathrm{s}}$, $V_A = 1$, and $V_B = 1$. Gluon fields are multipole expanded and depend only on the center of mass coordinate; they scale with the low-energy scales (T, m_D, α_{s}/r, Λ_{QCD}, ...) that are still dynamical in the EFT. The dots in the last line stand for higher-order terms in the multipole expansion.

A. Singlet and octet propagators

The free real-time singlet and octet static propagators at finite T are similar to the free static quark propagator (20), although singlet and octet are bosons:

$$\mathbf{S}^{\,\mathrm{singlet}}(p) = \begin{pmatrix} \frac{i}{p^0 + C_F \alpha_{V_s}/r + i\epsilon} & 0 \\ 2\pi\delta(p^0 + C_F \alpha_{V_s}/r) & \frac{-i}{p^0 + C_F \alpha_{V_s}/r - i\epsilon} \end{pmatrix} = \mathbf{U}^{(0)} \begin{pmatrix} \frac{i}{p^0 + C_F \alpha_{V_s}/r + i\epsilon} & 0 \\ 0 & \frac{-i}{p^0 + C_F \alpha_{V_s}/r - i\epsilon} \end{pmatrix} \mathbf{U}^{(0)}, \quad (56)$$

$$\mathbf{S}^{\,\mathrm{octet}}(p)_{ab} = \delta_{ab} \begin{pmatrix} \frac{i}{p^0 - \alpha_{V_o}/(2N_c r) + i\epsilon} & 0 \\ 2\pi\delta(p^0 - \alpha_{V_o}/(2N_c r)) & \frac{-i}{p^0 - \alpha_{V_o}/(2N_c r) - i\epsilon} \end{pmatrix} = \delta_{ab} \mathbf{U}^{(0)} \begin{pmatrix} \frac{i}{p^0 - \alpha_{V_o}/(2N_c r) + i\epsilon} & 0 \\ 0 & \frac{-i}{p^0 - \alpha_{V_o}/(2N_c r) - i\epsilon} \end{pmatrix} \mathbf{U}^{(0)}. \quad (57)$$

B. Nonthermal part of the singlet static potential

The contribution to the singlet static potential coming from the scale $1/r$ can be read from the Lagrangian (55); it is just the Coulomb potential, which in real-time formalism reads

$$\mathbf{V}_{\mathbf{s}}(r) = -C_F \frac{\alpha_{V_s}(1/r)}{r} \begin{pmatrix} 1 & 0 \\ 0 & -1 \end{pmatrix}, \quad (58)$$

where $\alpha_{V_s}(1/r)$ is a series in α_s: at leading order, $\alpha_{V_s}(1/r) = \alpha_s(1/r)$. Starting from order α_s^4, α_{V_s} is infrared divergent; these divergences, which appear at zero temperature, have been considered elsewhere [20] and will not matter here.

The matrix in (58) is such that

$$\begin{pmatrix} 1 & 0 \\ 0 & -1 \end{pmatrix} = [\mathbf{U}^{(0)}]^{-1} \begin{pmatrix} 1 & 0 \\ 0 & -1 \end{pmatrix} [\mathbf{U}^{(0)}]^{-1}. \tag{59}$$

Together with Eq. (22), this guarantees that

$$\mathbf{S}^{\text{singlet}}(p) = \begin{pmatrix} \frac{i}{p^0+i\epsilon} & 0 \\ 2\pi\delta(p^0) & \frac{-i}{p^0-i\epsilon} \end{pmatrix} \times \sum_{n=0}^{\infty} \left[(-i\mathbf{V}_s(r)) \begin{pmatrix} \frac{i}{p^0+i\epsilon} & 0 \\ 2\pi\delta(p^0) & \frac{-i}{p^0-i\epsilon} \end{pmatrix} \right]^n, \tag{60}$$

i.e., that, like at $T = 0$, the sum of all insertions of a potential exchange between a free quark and antiquark amounts to the propagator (56).

The singlet static potential does not get only contributions from the scale $1/r$, but, if the next relevant scales are the thermal ones, it will also get thermal contributions. These will be the subject of the following sections.

C. Chromoelectric correlator

In the paper, it will become necessary to calculate the chromoelectric correlator $\langle \vec{E}^a(t)\phi(t,0)^{\text{adj}}_{ab}\vec{E}^b(0)\rangle_T$, where $\phi(t,0)^{\text{adj}}_{ab}$ is a Wilson line in the adjoint representation connecting the points $(t,\vec{0})$ and $(0,\vec{0})$ by a straight line. Such a correlator enters each time we consider diagrams with two chromoelectric dipole insertions. In the real-time formalism, the chromoelectric correlator is a 2×2 matrix in the field indices 1 and 2. We shall write it as

$$\langle \vec{E}^a(t)\phi(t,0)^{\text{adj}}_{ab}\vec{E}^b(0)\rangle_T = (N_c^2-1)\int \frac{dk^0}{2\pi} e^{-ik^0 t} \int \frac{d^3k}{(2\pi)^3} \times ((k^0)^2 \mathbf{D}_{ii}(k) + \vec{k}^2 \mathbf{D}_{00}(k)), \tag{61}$$

where, at zeroth order in α_s, $\mathbf{D}_{\mu\nu}(k)$ is the free gluon propagator. In Coulomb gauge, the free gluon propagator has been given in Eqs. (36) and (37); since the chromoelectric correlator is a gauge invariant quantity the choice of the gauge does not matter. At zeroth order in α_s, the thermal part of $\langle \vec{E}^a(t)\phi(t,0)^{\text{adj}}_{ab}\vec{E}^b(0)\rangle_T$ is

$$\langle \vec{E}^a(t)\phi(t,0)^{\text{adj}}_{ab}\vec{E}^b(0)\rangle_T|_{\text{thermal part}} = (N_c^2-1)\int \frac{d^3k}{(2\pi)^3} 2|\vec{k}|\cos(|\vec{k}|t) n_B(|\vec{k}|) \begin{pmatrix} 1 & 1 \\ 1 & 1 \end{pmatrix}. \tag{62}$$

Note that for $t = 0$ Eq. (62) gives the thermal part of the gluon condensate in the weak-coupling regime:

$$\langle \vec{E}^a(0)\cdot\vec{E}^a(0)\rangle_T|_{\text{thermal part}} = (N_c^2-1)T^4\frac{\pi^2}{15}\begin{pmatrix} 1 & 1 \\ 1 & 1 \end{pmatrix}, \tag{63}$$

where we have used $\int_0^\infty dk k^3 n_B(k) = \pi^4 T^4/15$. Equation (63) agrees with the Stefan-Boltzmann law (see, for instance, [21]).

D. Thermal corrections to the singlet static potential

We calculate now the leading thermal contributions to the static potential assuming for definiteness that T and m_D are the next relevant scales after $1/r$, i.e., that the binding energy is much smaller than m_D. We will further assume that all other thermodynamical scales are much smaller than the binding energy, so that we can ignore them. We recall that from an EFT point of view, only energy scales larger than the binding energy contribute to the potential, which is the matching coefficient entering the Schrödinger equation of the bound state, while all energy scales contribute to physical observables such as, for instance, the static energy [10]. We will comment on the impact of degrees of freedom with energies and momenta of the order of the binding energy in Secs. IV E and IV F.

The calculation proceeds in two steps. The first step will be performed in Sec. IV D 1. It consists of integrating out from the pNRQCD Lagrangian (55) modes of energy and momentum of order T. This modifies pNRQCD into a new EFT where only modes with energy and momentum lower than the temperature are dynamical. For our purposes, it only matters that the pNRQCD Lagrangian gets additional contributions in the singlet and in the Yang-–Mills sectors. In the first sector, it is an additional contribution to the singlet static potential. In the second one, the additional contribution corresponds to the HTL Lagrangian [22].

The second step, which will be performed in Sec. IV D 2, consists of integrating out from the previous EFT modes of energy and momentum of order m_D. The resulting EFT will only have degrees of freedom that are dynamical at energy and momentum scales lower than the Debye mass. In the singlet sector, the EFT gets modified by a further additional contribution to the static potential.

In summary, if both T and m_D are much larger than the binding energy, the real-time Coulomb potential (58) gets two type of corrections $\delta\mathbf{V}_s(r)$. The first one comes from the scale T and the other one from the scale m_D.

1. Contributions from the scale T

The leading thermal correction $\delta\mathbf{V}_s(r)$ is induced by the dipole terms $\mathrm{O}^\dagger \vec{r}\cdot g\vec{E}\mathrm{S} + \mathrm{S}^\dagger \vec{r}\cdot g\vec{E}\mathrm{O}$ in the Lagrangian (55). It reads (see [19] for the $T = 0$ case):

$$[\delta\mathbf{V}_s(r)]_{11} = -ig^2\frac{T_F}{N_c}\frac{r^2}{d-1}\int_0^\infty dt e^{-it\Delta V} \times[\langle\vec{E}^a(t)\phi(t,0)^{\rm adj}_{ab}\vec{E}^b(0)\rangle_T]_{11} = -ig^2C_F\frac{r^2}{d-1}\mu^{4-d}\int\frac{d^dk}{(2\pi)^d} \times\frac{i}{-k^0-\Delta V+i\epsilon}[(k^0)^2\mathbf{D}_{ii}(k)+\vec{k}^2\mathbf{D}_{00}(k)]_{11}, \quad (64)$$

$$[\delta\mathbf{V}_s(r)]_{22} = -[\delta\mathbf{V}_s]^*_{11}, \quad (65)$$

$$[\delta\mathbf{V}_s(r)]_{12} = 0, \quad (66)$$

$$[\delta\mathbf{V}_s(r)]_{21} = ig^2C_F\frac{r^2}{d-1}\mu^{4-d}\int\frac{d^dk}{(2\pi)^d}2\pi\delta(-k^0-\Delta V) \times[(k^0)^2\mathbf{D}_{ii}(k)+\vec{k}^2\mathbf{D}_{00}(k)]_{21}, \quad (67)$$

where

$$\Delta V = \frac{1}{r}\left(\frac{\alpha_{V_o}}{2N_c}+C_F\alpha_{V_s}\right)\approx\frac{N_c\alpha_s}{2r}.$$

The corresponding Feynman diagram is shown in Fig. 5. Integrals over momenta have been regularized in dimensional regularization (d is the number of dimensions, μ is the compensating scale). In Eq. (64), $i/(-k^0-\Delta V+i\epsilon)$ arises from the 11 component of the static octet propagator; Eq. (66) vanishes because the 12 component of the static octet propagator vanishes and in Eq. (67), $2\pi\delta(-k^0-\Delta V)$ is the 21 component of the static octet propagator. Note that vertices of type 1 and 2 have opposite signs. Equation (65), which may also be read $[-i\delta\mathbf{V}_s(r)]_{22} = [-i\delta\mathbf{V}_s(r)]^*_{11}$, reflects the relation existing between the 11 and 22 components of the propagators in the real-time formalism.

We are interested in calculating the contribution to the integrals in Eqs. (64)–(67) from momenta $k\sim T$. Since $T\gg\Delta V$, we may expand in $\Delta V/T$. Moreover, at leading order, the propagators in Eqs. (64) and (67) are the free ones, $\mathbf{D}^{(0)}_{00}$ and $\mathbf{D}^{(0)}_{ii}$, given in Eqs. (36) and (37). However the leading-order thermal contribution, which would be of order $g^2r^2T^3$, vanishes

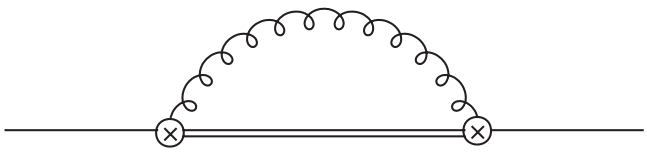

FIG. 5. The single continuous line stands for a singlet propagator, the double line for an octet propagator, the circle with a cross for a chromoelectric dipole vertex, and the curly line connecting the two circles with a cross for a chromoelectric correlator.

$$[\delta\mathbf{V}_s(r)]_{11} = -ig^2C_F\frac{r^2}{d-1}\mu^{4-d}\int\frac{d^dk}{(2\pi)^d}\frac{i}{-k^0+i\epsilon} \times(k^0)^2 4\pi\delta(k^2)n_B(|k^0|) = 0, \quad (68)$$

$$[\delta\mathbf{V}_s(r)]_{21} = ig^2C_F\frac{r^2}{d-1}\mu^{4-d}\int\frac{d^dk}{(2\pi)^d}2\pi\delta(-k^0) \times(k^0)^2 4\pi\delta(k^2)n_B(|k^0|) = 0. \quad (69)$$

Several next-to-leading-order corrections are possible, because several scales are still dynamical in the EFT: we may have corrections of relative order $\Delta V/T$, m_D/T, (rT), α_s, and so on.

(1) First, we consider corrections of order $\Delta V/k^0$ or higher to the quark-antiquark propagator, which contribute to order $g^2r^2T^3\times\Delta V/T$ or higher to $\delta\mathbf{V}_s(r)$:

$$[\delta\mathbf{V}_s(r)]_{11} = -ig^2C_F\frac{r^2}{d-1}\mu^{4-d}\int\frac{d^dk}{(2\pi)^d} \times\frac{i}{-k^0-\Delta V+i\epsilon} \times[(k^0)^2\mathbf{D}^{(0)}_{ii}(k)+\vec{k}^2\mathbf{D}^{(0)}_{00}(k)]_{11} = \frac{4}{3}C_F\frac{\alpha_s}{\pi}r^2T^2\Delta V f(\Delta V/T) - i\frac{2}{3}C_F\alpha_s r^2(\Delta V)^3 n_B(\Delta V), \quad (70)$$

$$[\delta\mathbf{V}_s(r)]_{21} = ig^2C_F\frac{r^2}{d-1}\mu^{4-d}\int\frac{d^dk}{(2\pi)^d} \times 2\pi\delta(-k^0-\Delta V) \times[(k^0)^2\mathbf{D}^{(0)}_{ii}(k)+\vec{k}^2\mathbf{D}^{(0)}_{00}(k)]_{21} = i\frac{4}{3}C_F\alpha_s r^2(\Delta V)^3 n_B(\Delta V) = -2i\,{\rm Im}[\delta\mathbf{V}_s(r)]_{11}, \quad (71)$$

where

$$f(z) = \int_0^\infty dx\frac{x^3}{e^x-1}{\rm P}\frac{1}{x^2-z^2}, \quad (72)$$

and P stands for the principal value. Since $T\gg\Delta V$, we can expand the above expressions in $\Delta V/T$ obtaining

$$\delta\mathbf{V}_s(r) = \frac{\pi}{9}N_cC_F\alpha_s^2rT^2\begin{pmatrix}1&0\\0&-1\end{pmatrix}+\cdots - \frac{i}{6}N_c^2C_F\alpha_s^3T\begin{pmatrix}1&0\\-2&1\end{pmatrix}+\cdots. \quad (73)$$

The dots stand for higher-order real and imaginary terms. We note that the matrices in Eq. (73) are such to be diagonalized by the matrix $[\mathbf{U}^{(0)}]^{-1}$: the first one is the same as in (59), the second one satisfies

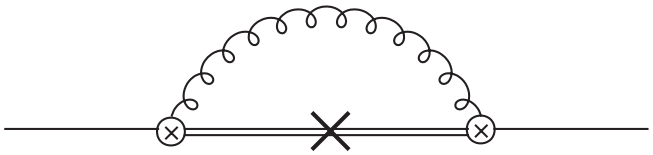

FIG. 6. Feynman diagram giving the leading-order real contribution to Eq. (70). The symbols are as in Fig. 5. The cross stands for a ΔV insertion in the octet propagator.

$$\begin{pmatrix} 1 & 0 \\ -2 & 1 \end{pmatrix} = [\mathbf{U}^{(0)}]^{-1} \begin{pmatrix} 1 & 0 \\ 0 & 1 \end{pmatrix} [\mathbf{U}^{(0)}]^{-1}. \tag{74}$$

The leading real contribution in Eq. (73) is of order $g^2 r^2 T^3 \times \Delta V/T$ and comes from the diagram shown in Fig. 6. The leading imaginary contribution in Eq. (73) is of order $g^2 r^2 T^3 \times (\Delta V/T)^2$ and comes from the diagram shown in Fig. 7. This imaginary part is a very peculiar feature of QCD. It originates from the fact that thermal fluctuations of the medium at short distances may destroy a color-singlet bound state in an octet quark-antiquark state and gluons. This process is kinematically not allowed at zero temperature where only static octets may decay into singlets with a leading-order width $\Gamma = N_c^2 \alpha_s^4/(12r)$. In some kinematical situations, the role of singlet-octet transitions in quarkonium-hadron scattering in strongly interacting matter has been discussed in Ref. [23].

Here we have assumed $T \gg \Delta V$. In the kinematical situation $T \sim \Delta V$, Eq. (70) would provide a contribution to the static energy rather than to the static potential of the quark-antiquark pair. This contribution will be discussed in Sec. IV E.

(2) Another source of next-to-leading-order corrections comes from next-to-leading-order corrections to the chromoelectric field correlator. Their contribution to the static potential at zero temperature has been considered in [24]. They also contribute at order $g^2 r^2 T^3 \times \alpha_s \sim g^2 r^2 T^3 \times (m_D/T)^2$ to the thermal part of the static potential. The chromoelectric correlator enters in the potential in the expression $\mu^{4-d} \int \frac{d^d k}{(2\pi)^d} \frac{i}{-k^0 + i\epsilon} [(k^0)^2 \mathbf{D}_{ii}(k) + \vec{k}^2 \mathbf{D}_{00}(k)]_{11}$. Since $i/(-k^0 + i\epsilon) = -i\mathrm{P}(1/k^0) + \pi\delta(-k^0)$ and $[(k^0)^2 \mathbf{D}_{ii}(k) + \vec{k}^2 \mathbf{D}_{00}(k)]_{11}$ is even in k^0, only the $\pi\delta(-k^0)$ component of the static quark-antiquark propagator contributes, therefore only the limit for $k^0 \to 0$ of $[(k^0)^2 \mathbf{D}_{ii}(k) + \vec{k}^2 \mathbf{D}_{00}(k)]$ matters. In order to evaluate it, it is convenient to perform the calculation first in temporal-axial gauge $A^0 = 0$. In this gauge, the chromoelectric field is simply $\vec{E} = -\partial_0 \vec{A}$. Hence all corrections to the chromoelectric correlator are encoded in the spatial part of the gluon propagator alone: at one loop the correction is provided entirely by the gluon self-energy. In temporal-axial gauge, from the transversality relation of the polarization tensor it follows that (compare with the expressions of the propagators in [16])

$$\lim_{k^0 \to 0} (k^0)^2 D_{ii}^{\mathrm{R,A}}(k) \Big|_{\text{temporal-axial gauge}} = \lim_{k^0 \to 0} i \frac{\vec{k}^2}{\vec{k}^2 + \Pi_{00}^{\mathrm{R,A}}(k)} \Big|_{\text{temporal-axial gauge}}. \tag{75}$$

Since in the $k^0 \to 0$ limit $\Pi_{00}^{\mathrm{R,A}}(k)$ is equal in Coulomb and temporal-axial gauge, we can also write that [compare with Eq. (50)]

$$\lim_{k^0 \to 0} (k^0)^2 D_{ii}^{\mathrm{R,A}}(k)|_{\text{temporal-axial gauge}} = \lim_{k^0 \to 0} \vec{k}^2 D_{00}^{\mathrm{R,A}}(k)|_{\text{Coulomb gauge}}. \tag{76}$$

The left-hand side is the only term of the chromoelectric correlator contributing to the potential in temporal-axial gauge: it may be evaluated by calculating the right-hand side in Coulomb gauge. At one loop, the right-hand side gets contribution from the gluon self-energy diagram shown in Fig. 8; hence, at next-to-leading order we can write

$$[\delta \mathbf{V}_s(r)]_{11} = -ig^2 C_F \frac{r^2}{d-1} \mu^{4-d} \int \frac{d^d k}{(2\pi)^d} \times \pi\delta(-k^0) \vec{k}^2 [\delta \mathbf{D}_{00}(k)]_{11}, \tag{77}$$

$$[\delta \mathbf{V}_s(r)]_{21} = ig^2 C_F \frac{r^2}{d-1} \mu^{4-d} \int \frac{d^d k}{(2\pi)^d} \times 2\pi\delta(-k^0) \vec{k}^2 [\delta \mathbf{D}_{00}(k)]_{21}, \tag{78}$$

where

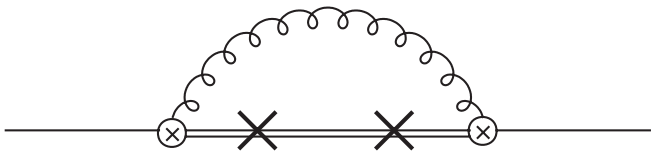

FIG. 7. Feynman diagram giving the leading-order imaginary contribution to Eq. (70). The symbols are as in Fig. 6.

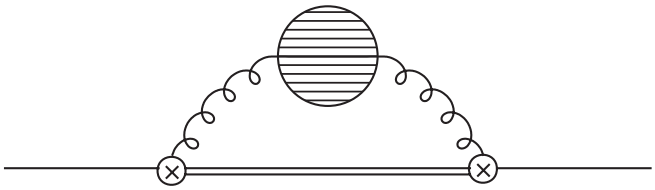

FIG. 8. The symbols are as in Fig. 5. The dashed blob stands for a one-loop self-energy insertion in the gluon propagator.

$$[\delta\mathbf{D}_{00}(k)]_{11} = \frac{\delta D^{\mathrm{R}}_{00}(k) + \delta D^{\mathrm{A}}_{00}(k)}{2} + \left(\frac{1}{2} + n_{\mathrm{B}}(k^0)\right) \times (\delta D^{\mathrm{R}}_{00}(k) - \delta D^{\mathrm{A}}_{00}(k)), \quad (79)$$

$$[\delta\mathbf{D}_{00}(k)]_{21} = (1 + n_{\mathrm{B}}(k^0))(\delta D^{\mathrm{R}}_{00}(k) - \delta D^{\mathrm{A}}_{00}(k)), \quad (80)$$

$$\delta D^{\mathrm{R,A}}_{00}(k) = -\frac{i}{\vec{k}^4}\Pi^{\mathrm{R,A}}_{00}(k), \quad (81)$$

and, the relevant limit for the gluon polarization $\Pi^{\mathrm{R,A}}_{00}(k)$ in Coulomb gauge is given by Eqs. (44) and (45). Finally, the correction to the real-time potential reads

$$\begin{aligned}\delta\mathbf{V}_{\mathbf{s}}(r) = &\left[-\frac{3}{2}\zeta(3)C_F\frac{\alpha_{\mathrm{s}}}{\pi}r^2Tm_D^2 + \frac{2}{3}\zeta(3)N_cC_F\alpha_{\mathrm{s}}^2r^2T^3\right]\begin{pmatrix}1 & 0\\ 0 & -1\end{pmatrix}\\ &+ i\left[\frac{C_F}{6}\alpha_{\mathrm{s}}r^2Tm_D^2\left(\frac{1}{\epsilon} + \gamma_E + \ln\pi - \ln\frac{T^2}{\mu^2} + \frac{2}{3} - 4\ln 2 - 2\frac{\zeta'(2)}{\zeta(2)}\right) + \frac{4\pi}{9}\ln 2N_cC_F\alpha_{\mathrm{s}}^2r^2T^3\right]\begin{pmatrix}1 & 0\\ -2 & 1\end{pmatrix}, \quad (82)\end{aligned}$$

where $\epsilon = (4-d)/2$, γ_E is the Euler gamma and ζ the Riemann zeta function [$\zeta(2) = \pi^2/6$]. Note that in Eq. (82), besides terms that are proportional to the Debye mass there are finite terms, both in the real and in the imaginary parts, that do not depend on it. Equation (82) contains an imaginary contribution. The origin of this contribution is different from the one in Eq. (73). The one here comes from the imaginary part in the gluon self-energy, which is due to the scattering of particles with momenta of order T in the thermal bath with spacelike gluons, $(k^0)^2 < |\vec{k}|^2$ (Landau damping) while the one in Eq. (73) signals the thermal breakup of a quark-antiquark color-singlet pair into an octet one.

The result in Eq. (82) is infrared divergent and, in an EFT language, calls for an opposite ultraviolet divergence from lower energy contributions: the two divergences should cancel in all physical observables. In the following section, we will show that the infrared divergence generated by the diagram in Fig. 8 when integrated over momenta of order T is canceled by an ultraviolet divergence in the same diagram when integrated over momenta of order m_D. For the purpose of the cancellation and the calculation of the static potential in the situation $1/r \gg T \gg m_D \gg \Delta V$ it is irrelevant how we regularize both divergent contributions, as long as they are regularized in the same way: the divergences as well as any scheme dependence cancel in the sum. However, it may be that expression (82) is used in intermediate calculations that require further regularizations. An example is the solution of the Schrödinger equation for quarkonium in a thermal medium when the kinetic energy of the bound state is larger than or of the same order as m_D so that the cancellation of the divergences does not occur at the level of the potential. In such a situation, it is important to provide divergent contributions in a standard regularization scheme. Equation (82) has been obtained by regularizing in dimensional regularization only the integral in k. This is not sufficient to qualify Eq. (82) as a standard dimensional regularization scheme result, which would also require the calculation of the gluon polarization tensor at order ϵ in the dimensional regularization expansion. This order, combined with the $1/\epsilon$ divergence of the integral in k, contributes to the finite part of (82). To our knowledge the expression of the gluon polarization tensor at order ϵ is not known in the literature and its calculation is beyond the purposes of this work. However, it may become necessary for a proper calculation of the quarkonium potential at short distances when the Debye mass is of the same order as or smaller than the kinetic energy.

(3) Finally, a source of higher-order contributions comes from higher-order terms in the multipole expansion. These are of two types. First, they may involve operators of higher order in the multipole expansion in the pNRQCD Lagrangian, such as, for example, the operator $\frac{1}{24}\mathrm{Tr}\{\mathrm{O}^\dagger r^i r^j r^k g D^i D^j E^k \mathrm{S}\}$. However, the contribution of this operator vanishes for reasons similar to the ones that led to the vanishing of the leading-order thermal contribution in Eqs. (68) and (69). Second, they may involve diagrams with three or more insertions of the operators $\mathrm{Tr}\{\mathrm{O}^\dagger \vec{r}\cdot g\vec{E}\mathrm{S}\}$ or $\mathrm{Tr}\{\mathrm{O}^\dagger \vec{r}\cdot g\vec{E}\mathrm{O}\}$. They contribute to order $g^2r^2T^3 \times g^2rT$ or higher to the thermal part of the static potential and hence are suppressed by at least a factor rT with respect to the corrections considered in the previous paragraph. We will neglect them in the following.

2. Contributions from the scale m_D

In the previous section, having integrated out T has led to a new EFT, which in the Yang-Mills sector coincides with the HTL EFT and in the singlet sector shows a potential that is the sum of the terms (58), (73), and (82). In the weak-coupling regime, the Debye mass m_D, which is given by Eq. (48), is smaller than the temperature. We assume that m_D is the most relevant scale in the new EFT. The leading contributions to the static potential from the scale m_D originate from the diagram shown in

Fig. 5 when integrated over momenta $k \sim m_D$. They are given by

$$[\delta \mathbf{V_s}(r)]_{11} = -ig^2 C_F \frac{r^2}{d-1} \mu^{4-d} \int \frac{d^d k}{(2\pi)^d} \frac{i}{-k^0 + i\epsilon} \times [(k^0)^2 \mathbf{D}_{ii}(k) + \vec{k}^2 \mathbf{D}_{00}(k)]_{11}$$
$$= -ig^2 C_F \frac{r^2}{d-1} \mu^{4-d} \int \frac{d^d k}{(2\pi)^d} \times \pi \delta(-k^0)[(k^0)^2 \mathbf{D}_{ii}(k) + \vec{k}^2 \mathbf{D}_{00}(k)]_{11}, \quad (83)$$

$$[\delta \mathbf{V_s}(r)]_{22} = -[\delta \mathbf{V_s}]^*_{11}, \quad (84)$$

$$[\delta \mathbf{V_s}(r)]_{12} = 0, \quad (85)$$

$$[\delta \mathbf{V_s}(r)]_{21} = ig^2 C_F \frac{r^2}{d-1} \mu^{4-d} \int \frac{d^d k}{(2\pi)^d} 2\pi \delta(-k^0) \times [(k^0)^2 \mathbf{D}_{ii}(k) + \vec{k}^2 \mathbf{D}_{00}(k)]_{21}, \quad (86)$$

where $\mathbf{D}_{\mu\nu}(k)$ is now the HTL resummed propagator. After integration in k^0 only $\mathbf{D}_{00}(0, \vec{k})$ contributes, the expression of which can be found in (53). Substituting and performing the dimensional integrals, we obtain

$$\delta \mathbf{V_s}(r) = \frac{C_F}{6} \alpha_s r^2 m_D^3 \begin{pmatrix} 1 & 0 \\ 0 & -1 \end{pmatrix} - i \frac{C_F}{6} \alpha_s r^2 T m_D^2 \left(\frac{1}{\epsilon} - \gamma_E + \ln \pi + \ln \frac{\mu^2}{m_D^2} + \frac{5}{3} \right) \times \begin{pmatrix} 1 & 0 \\ -2 & 1 \end{pmatrix}. \quad (87)$$

Equation (87) shows that the scale m_D contributes at order $g^2 r^2 m_D^3$ to the real part of the potential and at order $g^2 r^2 T m_D^2$ to the imaginary one.

The Debye mass effectively plays the role of a gluon mass; in this sense, the real part of (87) agrees with a result that can be found in [19]. The imaginary part originates, as the one in Eq. (82), from the imaginary part of the gluon self-energy. It shows an ultraviolet divergence. This cancels against the infrared divergence of Eq. (82), which, we recall, comes from the diagram in Fig. 8 when integrated over momenta of order T. We have already commented on this cancellation at the end of the previous section; we will add further specifications in Sec. IV F.

E. Singlet static energy for $T \lesssim \Delta V$

If $T \sim \Delta V$ there are no temperature-dependent corrections to the potential, but Eq. (70) gives the leading thermal correction to the pole of the color-singlet propagator. The real part of the pole provides the static energy of a color-singlet quark-antiquark pair, whose leading thermal part is

$$\delta E_s = \frac{2}{3} N_c C_F \frac{\alpha_s^2}{\pi} r T^2 f(N_c \alpha_s/(2rT)), \quad (88)$$

where the function f has been defined in (72). Minus twice the imaginary part of the pole provides the color-singlet thermal decay width, whose leading contribution, due to the decay of a static quark-antiquark color singlet into a quark-antiquark color octet, is

$$\Gamma = \frac{N_c^3 C_F}{6} \frac{\alpha_s^4}{r} n_B(N_c \alpha_s/(2r)). \quad (89)$$

In the situation $T \ll \Delta V$, the thermal width is exponentially suppressed, while the thermal contribution to the static energy becomes

$$\delta E_s = -\frac{8}{45} \pi^3 \frac{C_F}{N_c} r^3 T^4 = -\frac{4}{3} \pi \frac{C_F}{N_c} r^3 \langle \vec{E}^a(0) \cdot \vec{E}^a(0) \rangle_T |_{\text{thermal part}}. \quad (90)$$

Equation (90) agrees with the analogous expression for the leading gluon condensate correction to the quark-antiquark static energy at zero temperature that was derived in [25].

F. Summary and comments

As in the zero temperature case also in a thermal bath, the computation of the real-time potential between a static quark-antiquark pair requires integrating out all modes of energy and momentum larger than ΔV. Modes of energy or momentum of order ΔV or smaller enter in physical observables, but, since they depend on the binding energy, do not belong to a proper EFT definition of the potential [10].

If $1/r \gg T \gg m_D \gg \Delta V$ and in the weak-coupling regime, the static potential of a quark-antiquark pair is obtained by adding Eqs. (58), (73), (82), and (87). In its diagonal form, it is given by

$$\mathbf{V_s}(r) = [\mathbf{U}^{(0)}]^{-1} \begin{pmatrix} V_s(r) & 0 \\ 0 & -V_s(r)^* \end{pmatrix} [\mathbf{U}^{(0)}]^{-1}, \quad (91)$$

where

$$V_s(r) = -C_F \frac{\alpha_{V_s}(1/r)}{r} + \frac{\pi}{9} N_c C_F \alpha_s^2 r T^2 - \frac{3}{2} \zeta(3) C_F \frac{\alpha_s}{\pi} r^2 T m_D^2 + \frac{2}{3} \zeta(3) N_c C_F \alpha_s^2 r^2 T^3 + \frac{C_F}{6} \alpha_s r^2 m_D^3 + \cdots + i \Big[-\frac{N_c^2 C_F}{6} \alpha_s^3 T + \frac{C_F}{6} \alpha_s r^2 T m_D^2 \Big(2\gamma_E - \ln \frac{T^2}{m_D^2} - 1 - 4 \ln 2 - 2 \frac{\zeta'(2)}{\zeta(2)} \Big) + \frac{4\pi}{9} \ln 2 N_c C_F \alpha_s^2 r^2 T^3 \Big] + \cdots. \quad (92)$$

The leading term is provided by the Coulomb part: $-C_F \alpha_s/r$. In the real part, the first thermal correction is

of order $g^2r^2T^3 \times \Delta V/T$, the second and third ones are of order $g^2r^2T^3 \times (m_D/T)^2$, and the last one is of order $g^2r^2m_D^3$. The correction proportional to $\alpha_s r^2 m_D^3$ is suppressed by m_D/T with respect to the one proportional to $\alpha_s r^2 T m_D^2$ and may be neglected. In the imaginary part, the first term is of order $g^2r^2T^3 \times (\Delta V/T)^2$ and the other ones are of order $g^2r^2T^3 \times (m_D/T)^2$. The dots in (92) stand for higher-order real and imaginary terms. Temperature-dependent higher-order terms are suppressed by powers of $\Delta V/T$, m_D/T, rT, $\Delta V/m_D$, and rm_D.

The imaginary part of $V_s(r)$ has two origins. The first term comes from the thermal breakup of a quark-antiquark color-singlet state into a color-octet state. The other terms come from imaginary contributions to the gluon self-energy that may be traced back to the Landau damping phenomenon. Both are thermal effects: the first one is specific of the non-Abelian nature of QCD, and the second one would also show up in QED, although in QED the photon polarization tensor would get only fermionic contributions. Having assumed $T \gg m_D \gg \Delta V$, the term due to the singlet to octet breakup is suppressed by $(\Delta V/m_D)^2$ with respect to the imaginary gluon self-energy contributions, which provide therefore the parametrically leading contribution to the imaginary part of the potential.

The thermal part of Eq. (92) is finite because, under the condition $1/r \gg T \gg m_D \gg \Delta V$, it provides the leading thermal contribution to the real-time energy and to the decay width of a static quark and antiquark pair in a color-singlet configuration. Note, however, that the non-thermal part of the potential, α_{V_s}, develops infrared divergences starting from order α_s^4, which eventually cancel in physical quantities against contributions from the scale ΔV. These have been most recently considered in [24]. If $1/r \gg T \gg \Delta V \gtrsim m_D$, the static potential is the sum of Eqs. (58), (73), and (82). The thermal part is infrared divergent. Divergences cancel in physical observables against thermal contributions coming from the scale m_D. Finally, if $1/r \gg \Delta V \gtrsim T$, the static potential is just its Coulomb part (58). Thermal contributions affect physical observables through loop corrections that involve momenta or energies of the order of the binding energy or smaller, but do not modify the potential. In this case, the leading thermal effect on the static energy of the color-singlet quark-antiquark pair can be read in (88) and the leading thermal width, which is due to the singlet to octet breakup phenomenon, in (89).

Our result is also relevant for the case of a quark and antiquark with a large but finite mass m. This would correspond to the actual case of heavy quarkonium in a thermal medium. However, in the case of finite mass, the relevant scales of the bound state are dynamical and the above discussion gets modified accordingly. For a comprehensive review in the $T = 0$ case we refer to [10]. Bound states of heavy quarks are characterized by the energy scales m, mv, and mv^2, where v is the relative velocity of the heavy quarks: mv is of the order of the inverse size of the bound state and mv^2 is of the order of the kinetic or binding energy. The equation of motion of the quark-antiquark bound state reduces in the nonrelativistic limit to the Schrödinger equation. The potential is the interaction term entering the Schrödinger equation. Only modes of energy and momentum larger than mv^2 contribute to the potential. With these specifications, Eq. (92) provides the static potential of a heavy quarkonium in a thermal medium under the condition $m \gg mv \gg T \gg m_D \gg mv^2$. If $m \gg mv \gg T \gg mv^2 \gtrsim m_D$, the heavy quarkonium static potential is given by the sum of Eqs. (58), (73), and (82) only. The potential turns out to be infrared divergent also in its thermal part and the comment at the end of paragraph (2) of Sec. IV D 1 applies. The divergence will eventually cancel in physical quantities against contributions coming from the scale mv^2 or lower. If $m \gg mv \gg mv^2 \gtrsim T \gg m_D$, the heavy quarkonium static potential is just the Coulomb potential (58) and thermal corrections enter physical quantities in loop involving momenta at the scale mv^2 or lower.

In the next section, we provide a derivation of Eq. (92) that does not make use of the EFT language and follows directly from a calculation of the potential in perturbative QCD.

V. SHORT-DISTANCE THERMAL CORRECTIONS TO THE POTENTIAL IN PERTURBATIVE QCD

In this section, we ask the question of what would be the origin of the thermal part of the potential given by Eq. (92) if we would not introduce any EFT treatment, but simply perform a calculation in perturbative QCD under the condition that $1/r \gg T$ and where the binding energy is much smaller than m_D. The answer is that the thermal part of (92) would originate from the longitudinal-gluon exchange, with a self-energy insertion, between a static quark and a static antiquark shown in Fig. 9 and from the box diagram shown in Fig. 11.

We first consider the diagram in Fig. 9, which contributes to the physical 11 component of the static potential by

$$[\delta \mathbf{V}_s(r)]_{11} = \mu^{4-d} \int \frac{d^{d-1}k}{(2\pi)^{d-1}} e^{-i\vec{k}\cdot\vec{r}} g^2 C_F [i\delta \mathbf{D}_{00}(0,\vec{k})]_{11}, \tag{93}$$

where $\delta \mathbf{D}_{00}(k)$ is defined in Eqs. (79)–(81) and depends on the gluon polarization $\Pi_{00}^{\mathrm{R,A}}$. Note that we have set to zero the fourth component of the momentum in the longitudinal gluon: corrections would be suppressed by powers of $k^0/|\vec{k}| \sim V_s r$ or V_s/T or V_s/m_D. Equation (93) gets contributions from different momentum regions.

(1) The first momentum region is $|\vec{k}| \sim 1/r$. The thermal contribution to the longitudinal-gluon polarization tensor when $|\vec{k}| \sim 1/r \gg T$ is provided by Eq. (54), which, substituted in Eq. (93), gives (the

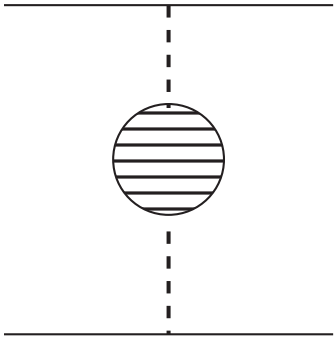

FIG. 9. Longitudinal-gluon exchange between a static quark and a static antiquark; the dashed blob stands for the gluon self-energy.

integral is finite, hence $d = 4$)

$$[\delta \mathbf{V}_{\mathbf{s}}(r)]_{11} = \int \frac{d^3k}{(2\pi)^3} e^{-i\vec{k}\cdot\vec{r}} \left(-C_F \frac{4\pi\alpha_s}{\vec{k}^4}\right) \frac{N_c g^2 T^2}{18} = \frac{\pi}{9} N_c C_F \alpha_s^2 r T^2, \tag{94}$$

where we have used that the Fourier transform of $4\pi/\vec{k}^4$ is $-r/2$. Equation (94) agrees with the real part of Eq. (73).

(2) A second momentum region is $|\vec{k}| \sim T$. Since $T \ll 1/r$, under the condition $|\vec{k}| \sim T$ we may expand the exponential $e^{-i\vec{k}\cdot\vec{r}}$ in (93):

$$[\delta \mathbf{V}_{\mathbf{s}}(r)]_{11} = \mu^{4-d} \int \frac{d^{d-1}k}{(2\pi)^{d-1}} \left(1 - \frac{(\vec{k}\cdot\vec{r})^2}{2} + \cdots\right) g^2 C_F [i\delta \mathbf{D}_{00}(0, \vec{k})]_{11}. \tag{95}$$

The first term in the expansion corresponds to a mass correction and cancels against twice the thermal contribution of the static quark self-energy with a gluon self-energy insertion; see Fig. 10. The second term coincides with the expression in Eq. (77) and gives the same result as (82).

(3) Finally, a third momentum region is $|\vec{k}| \sim m_D$. The contribution to the potential is like Eq. (95), but now $|\vec{k}| \sim m_D \ll T$ and the correct expression for $\mathbf{D}_{00}(0, \vec{k})$ is the HTL resummed propagator given in (53). The first term in the expansion corresponds to a mass correction, which this time comes from the scale m_D and cancels against twice the contribution of the static quark self-energy, see Fig. 1, when the loop momentum is of order m_D and a HTL resummed gluon propagator is used. The second term gives the same result as (87).

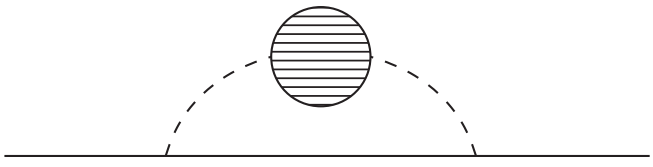

FIG. 10. Gluon self-energy correction to the one-loop self-energy diagram of a static quark.

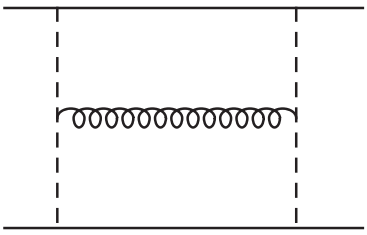

FIG. 11. Box diagram: the upper line represents a static quark and the lower one a static antiquark.

We consider now the diagram of Fig. 11, which contributes to the physical 11 component of the static potential by (we write the thermal part only)

$$[\delta \mathbf{V}_{\mathbf{s}}(r)]_{11} = \int \frac{d^3k}{(2\pi)^3} e^{-i\vec{k}\cdot\vec{r}} \Bigg[i N_c^2 C_F g^6 \int \frac{d^4p}{(2\pi)^4} \int \frac{d^4q}{(2\pi)^4} \times p^i (k^j - p^j) \frac{i}{-p^0 + i\epsilon} \frac{i}{p^0 - q^0 + i\epsilon} \times \left(\delta_{ij} - \frac{q^i q^j}{\vec{q}^2}\right) 2\pi\delta(q^2) n_{\mathrm{B}}(|q^0|) \frac{i}{\vec{p}^2} \frac{i}{|\vec{p} - \vec{q}|^2} \times \frac{i}{|\vec{k} - \vec{p}|^2} \frac{i}{|\vec{k} - \vec{p} + \vec{q}|^2} \Bigg]. \tag{96}$$

The imaginary part of the integral comes from the real part

$$\mathrm{Re} \int \frac{dp^0}{2\pi} \frac{i}{-p^0 + i\epsilon} \frac{i}{p^0 - q^0 + i\epsilon} = \mathrm{Re} \frac{i}{-q^0 + i\epsilon} = \pi\delta(-q^0),$$

which inserted in (96) gives the imaginary part of (73). The result is exact and does not rely on any expansion in the kinematical variables.

The sum of the contributions coming from the three momentum regions in the integral (93) and from the imaginary part of (96) gives Eq. (92). We note that also the calculation in perturbative QCD shows that the imaginary part of Eq. (73) has a different origin from the other ones: it comes from the box diagram of Fig. 11, which describes a singlet-to-octet-to-singlet transition, while the other ones come from the gluon self-energy diagram of Fig. 9.

VI. BOUND STATES FOR $1/r \ll T$

In this section, we consider bound states made of a static quark and antiquark in a thermal bath at distances such that $1/r \ll T$. We still keep that T, $1/r$, and m_D are perturbative scales. We further neglect other thermodynamical scales.

Under the above condition, the first scale to integrate out from QCD is the temperature T. At one loop, this was done in Sec. III. Integrating out T leads in the Yang-Mills sector to the HTL Lagrangian [22]. In the heavy-quark sector, one-loop contributions vanish in the static limit. At two loop, see for instance the diagram in Fig. 10, there may be effects. These are of order $\alpha_s^2 T \sim \alpha_s T (m_D/T)^2 \sim \alpha_s m_D (m_D/T)$ and will be neglected in the following where we shall concentrate on the leading contribution coming from the scale m_D.

The next scale to integrate out is $1/r$. We assume $1/r \gtrsim m_D$, and integrate out both scales $1/r$ and m_D at the same time. We shall specialize to the case $1/r \gg m_D$ in Sec. VI E.

A. Singlet and octet propagators

After integrating out the scales $1/r \gtrsim m_D$ it may be convenient to introduce quark-antiquark fields in analogy with what was done in previous sections. The real-time quark-antiquark propagator, $\mathbf{S}(p)$, is a 2×2 matrix obtained by matching equal-time quark and antiquark propagators such that $[\mathbf{S}(p)]_{ij}$ provides the propagator of a quark-antiquark pair of type i into a quark-antiquark pair of type j. The explicit expressions of the free color-singlet and color-octet quark-antiquark propagators are similar to those derived in Sec. IV A:

$$\mathbf{S}^{\text{singlet}(0)}(p) = \begin{pmatrix} \frac{i}{p^0+i\epsilon} & 0 \\ 2\pi\delta(p^0) & \frac{-i}{p^0-i\epsilon} \end{pmatrix} = \mathbf{U}^{(0)} \begin{pmatrix} \frac{i}{p^0+i\epsilon} & 0 \\ 0 & \frac{-i}{p^0-i\epsilon} \end{pmatrix} \mathbf{U}^{(0)}, \tag{97}$$

$$\mathbf{S}^{\text{octet}(0)}(p)_{ab} = \delta_{ab} \begin{pmatrix} \frac{i}{p^0+i\epsilon} & 0 \\ 2\pi\delta(p^0) & \frac{-i}{p^0-i\epsilon} \end{pmatrix} = \delta_{ab} \mathbf{U}^{(0)} \begin{pmatrix} \frac{i}{p^0+i\epsilon} & 0 \\ 0 & \frac{-i}{p^0-i\epsilon} \end{pmatrix} \mathbf{U}^{(0)}. \tag{98}$$

Singlet and octet fields have been normalized as in Sec. IV.

Thermal contributions from the scales $1/r \gtrsim m_D$ modify the quark-antiquark propagator. In particular, the singlet propagator gets the form

$$\mathbf{S}^{\text{singlet}}(p) = \begin{pmatrix} \frac{i}{p^0-\delta m-V_s(r)+i\epsilon} & 0 \\ \frac{i}{p^0-\delta m-V_s(r)+i\epsilon} - \frac{i}{p^0-\delta m^*-V_s^*(r)-i\epsilon} & \frac{-i}{p^0-\delta m^*-V_s^*(r)-i\epsilon} \end{pmatrix} = \mathbf{S}^{\text{singlet}(0)}(p) + \mathbf{S}^{\text{singlet}(0)}(p)[-i\delta\mathbf{m} - i\mathbf{V_s}]\mathbf{S}^{\text{singlet}(0)}(p) + \cdots, \tag{99}$$

where in the last line we have expanded with respect to δm and V_s and introduced the 2×2 matrices:

$$\delta\mathbf{m} = \begin{pmatrix} \delta m & 0 \\ -2i\,\mathrm{Im}\delta m & -\delta m^* \end{pmatrix} = [\mathbf{U}^{(0)}]^{-1} \begin{pmatrix} \delta m & 0 \\ 0 & -\delta m^* \end{pmatrix} [\mathbf{U}^{(0)}]^{-1}, \tag{100}$$

$$\mathbf{V_s} = \begin{pmatrix} V_s & 0 \\ -2i\,\mathrm{Im}V_s & -V_s^* \end{pmatrix} = [\mathbf{U}^{(0)}]^{-1} \begin{pmatrix} V_s & 0 \\ 0 & -V_s^* \end{pmatrix} [\mathbf{U}^{(0)}]^{-1}. \tag{101}$$

B. Matching the mass term δm

The static quark (antiquark) self-energy at one loop is shown in Fig. 1. In the case considered here, the loop momentum is of order m_D and the HTL resummed gluon propagator is used. We match in the real-time formalism the self-energy diagram (normalized in color space) with the second term in the expansion (99), $\mathbf{S}^{\text{singlet}(0)}(p) \times [-i\delta\mathbf{m}]\mathbf{S}^{\text{singlet}(0)}(p)$, obtaining

$$[\delta\mathbf{m}]_{11} = i(ig)^2 C_F \mu^{4-d} \int \frac{d^dk}{(2\pi)^d} \left[\frac{i}{-k^0+i\epsilon} - \frac{i}{-k^0-i\epsilon} \right] \times [\mathbf{D}_{00}(k)]_{11} = i(ig)^2 C_F \mu^{4-d} \int \frac{d^dk}{(2\pi)^d} 2\pi\delta(-k^0)[\mathbf{D}_{00}(k)]_{11} = -C_F \alpha_s (m_D + iT), \tag{102}$$

$$[\delta\mathbf{m}]_{22} = -[\delta\mathbf{m}]_{11}^*, \tag{103}$$

$$[\delta\mathbf{m}]_{12} = 0, \tag{104}$$

$$[\delta\mathbf{m}]_{21} = ig^2 C_F \mu^{4-d} \int \frac{d^dk}{(2\pi)^d} [2\pi\delta(-k^0) + 2\pi\delta(-k^0)] \times [\mathbf{D}_{00}(k)]_{21} = 2iC_F \alpha_s T, \tag{105}$$

where $i/(-k^0+i\epsilon)$ and $-i/(-k^0-i\epsilon)$ are the 11 components of the static quark and antiquark propagators, respectively, $2\pi\delta(-k^0)$ is the 21 component of both static quark and antiquark propagators and we have added the contributions from the quark and the antiquark; Eq. (104) vanishes because the component 12 of the heavy quark and antiquark propagators vanishes; see Eqs. (20) and (21). $\mathbf{D}_{00}(k)$ is the longitudinal HTL resummed gluon propagator, whose expression for $k^0 = 0$ is given in Eq. (53).

The matrix $\delta\mathbf{m}$ has indeed the form (100); it is diagonalized by the matrix $[\mathbf{U}^{(0)}]^{-1}$ and δm is given by

$$\delta m = -C_F\alpha_s(m_D + iT). \tag{106}$$

The real part of δm corresponds to the free energy of two isolated static quarks in the imaginary-time formalism, which was first calculated in Ref. [26] (for further discussions see Ref. [27]). The imaginary part of δm is minus twice the damping rate of an infinitely heavy fermion [28].

C. Matching the singlet static potential V_s

The matrix elements $[\mathbf{V_s}]_{ij}$ are obtained by matching in real time one-gluon exchange diagrams that transform a quark-antiquark pair of type i into a quark-antiquark pair of type j with the third term in the expansion (99), $\mathbf{S}^{\text{singlet}(0)}(p)[-i\mathbf{V_s}]\mathbf{S}^{\text{singlet}(0)}(p)$. More precisely, by matching the diagram of Fig. 12 with $[\mathbf{S}^{\text{singlet}(0)}(p)]_{11}[-i\mathbf{V_s}]_{11}\times[\mathbf{S}^{\text{singlet}(0)}(p)]_{11}$, the diagram of Fig. 13 with $[\mathbf{S}^{\text{singlet}(0)}(p)]_{22}[-i\mathbf{V_s}]_{22}[\mathbf{S}^{\text{singlet}(0)}(p)]_{22}$, the diagrams of Fig. 14 with $[\mathbf{S}^{\text{singlet}(0)}(p)]_{1i}[-i\mathbf{V_s}]_{ij}[\mathbf{S}^{\text{singlet}(0)}(p)]_{j2}$, and the diagrams of Fig. 15 with $[\mathbf{S}^{\text{singlet}(0)}(p)]_{2i}[-i\mathbf{V_s}]_{ij}\times[\mathbf{S}^{\text{singlet}(0)}(p)]_{j1}$, we obtain

$$\begin{aligned}[\mathbf{V_s}(r)]_{11} &= \int\frac{d^3k}{(2\pi)^3}e^{-i\vec{k}\cdot\vec{r}}ig^2C_F[\mathbf{D}_{00}(0,\vec{k})]_{11}\\ &= \int\frac{d^3k}{(2\pi)^3}e^{-i\vec{k}\cdot\vec{r}}\Bigg(-C_F\frac{4\pi\alpha_s}{\vec{k}^2+m_D^2}\\ &\quad + iC_F\frac{T}{|\vec{k}|}m_D^2\frac{4\pi^2\alpha_s}{(\vec{k}^2+m_D^2)^2}\Bigg),\end{aligned} \tag{107}$$

$$[\mathbf{V_s}(r)]_{22} = -[\mathbf{V_s}(r)]_{11}^*, \tag{108}$$

$$[\mathbf{V_s}(r)]_{12} = 0, \tag{109}$$

$$\begin{aligned}[\mathbf{V_s}(r)]_{21} &= \int\frac{d^3k}{(2\pi)^3}e^{-i\vec{k}\cdot\vec{r}}i(-g^2)C_F([\mathbf{D}_{00}(0,\vec{k})]_{12}\\ &\quad + [\mathbf{D}_{00}(0,\vec{k})]_{21})\\ &= -2i\text{Im}[\mathbf{V_s}(r)]_{11},\end{aligned} \tag{110}$$

where the longitudinal HTL resummed gluon propagator, $\mathbf{D}_{00}(0,\vec{k})$, given in Eq. (53), comes from expanding in the external energy, which is much smaller than the typical momentum $\sim 1/r$.

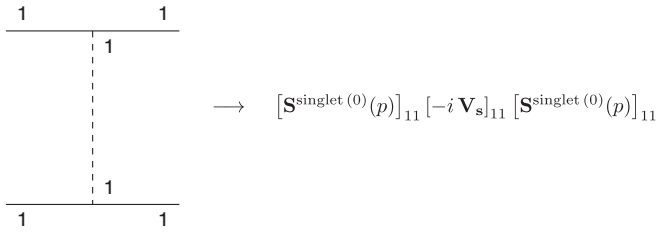

FIG. 12. Matching condition for $[-i\mathbf{V_s}]_{11}$; the numbers label the type 1 and 2 propagators. All entries in a vertex are of the same type. Vertices of type 1 and 2 have opposite signs.

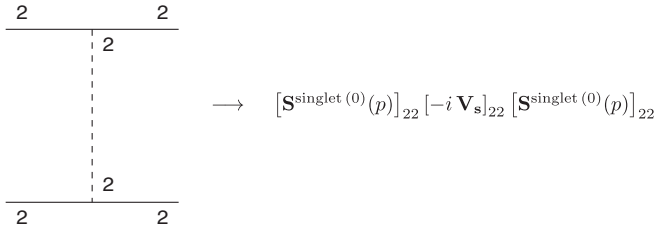

FIG. 13. Matching condition for $[-i\mathbf{V_s}]_{22}$.

The matching conditions of Figs. 12 and 13 fix $[\mathbf{V_s}(r)]_{11}$ and $[\mathbf{V_s}(r)]_{22}$ as in Eqs. (107) and (108), respectively. In Figs. 14 and 15 the first two diagrams cancel in the matching against the terms $i=j=1$ and $i=j=2$ in the sum on the right-hand side. In the case of Fig. 14, the last two diagrams vanish, because the 12 component of the static quark propagator vanishes, leading to Eq. (109); while in the case of Fig. 15, the last two diagrams give $[\mathbf{V_s}(r)]_{21}$ as in Eq. (110).

The matrix $\mathbf{V_s}$ has indeed the form (101); it is diagonalized by the matrix $[\mathbf{U}^{(0)}]^{-1}$ and V_s is given by

$$\begin{aligned}V_s(r) &= \int\frac{d^3k}{(2\pi)^3}e^{-i\vec{k}\cdot\vec{r}}\Bigg(-C_F\frac{4\pi\alpha_s}{\vec{k}^2+m_D^2}\\ &\quad + iC_F\frac{T}{|\vec{k}|}m_D^2\frac{4\pi^2\alpha_s}{(\vec{k}^2+m_D^2)^2}\Bigg)\\ &= -C_F\frac{\alpha_s}{r}e^{-m_Dr} + iC_F\alpha_sT\frac{2}{rm_D}\\ &\quad\times\int_0^\infty dx\frac{\sin(m_Drx)}{(x^2+1)^2}.\end{aligned} \tag{111}$$

The expression of $V_s(r)$, which we have derived here in real-time formalism, agrees with the analogous expression derived in imaginary-time formalism, after analytical continuation, in [5]. It should be emphasized that under the condition $1/r \sim m_D$ the real part of (111) is of order $\alpha_s m_D$, hence subleading with respect to the imaginary part, which is of order $\alpha_s T$: the quark-antiquark pair decays before forming the bound state, whose typical time scale is proportional to the inverse of the real part of the potential.

Note that the short-distance expansion of Eq. (111) would give, up to order r^0, the Coulomb potential and an r-independent term, $C_F\alpha_s(m_D + iT)$, which would cancel the mass term derived in (106). In the kinematical situation discussed here, this reflects the analogous cancellation between the mass correction and the potential correction induced by the scale m_D discussed in paragraph (3) of Sec. V.

In this section, we have assumed that the singlet propagator has the form (99) and verified that this is indeed the case by performing the matching. We could also have

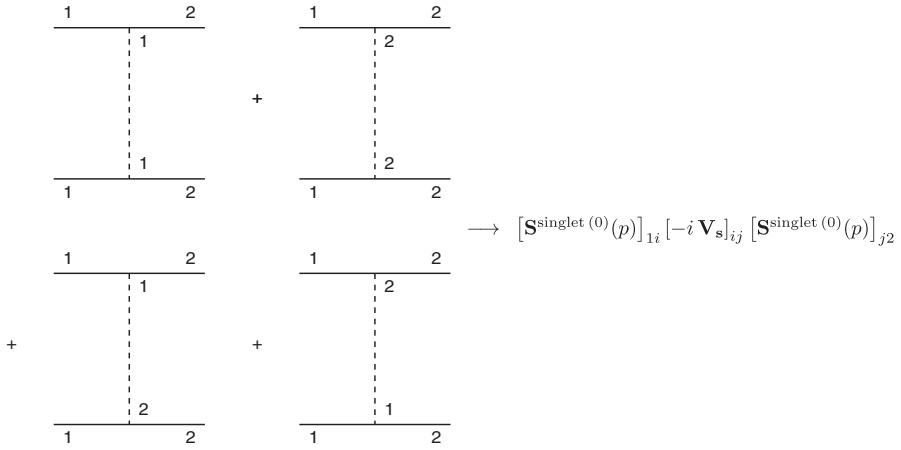

FIG. 14. Matching condition for $[-i\mathbf{V_s}]_{12}$.

proceeded with the reverse logic used in the rest of the paper: by matching $\delta\mathbf{m}$ and $\delta\mathbf{V_s}$ we would have realized that these matrices are diagonalized by $[\mathbf{U}^{(0)}]^{-1}$, hence, that they fulfill Eq. (60) and give rise to the resummed propagator (99).

D. Singlet static energy for $1/r \sim m_D$

Adding the real parts of Eqs. (106) and (111) gives the leading static quark-antiquark energy for $1/r \sim m_D$:

$$E_s = -C_F\alpha_s m_D - C_F\frac{\alpha_s}{r}e^{-m_D r}, \tag{112}$$

and the imaginary parts of Eqs. (106) and (111) provide the leading static quark-antiquark thermal decay width:

$$\Gamma = 2C_F\alpha_s T\left[1 - \frac{2}{rm_D}\int_0^\infty dx\frac{\sin(m_D rx)}{(x^2+1)^2}\right]. \tag{113}$$

The thermal width originates from the imaginary part of the gluon self-energy. Singlet to octet transitions contribute to the decay width as well and the leading contribution is provided by the diagram of Fig. 11, which gives [see the imaginary part of (73)]: $\delta\Gamma = \frac{1}{3}N_c^2 C_F\alpha_s^3 T$. This contribution is parametrically suppressed by a factor α_s^2, whose natural scale is of order $1/r$, with respect to the one in (113). Note, however, that $\delta\Gamma$ may be numerically as large as 50% of Γ for $\alpha_s \approx 0.3$ and even larger than Γ for $\alpha_s \approx 0.5$; see also Fig. 16.

The static energy given by Eq. (112) coincides with the leading-order result [27] of the so-called singlet free energy first introduced by Nadkarni [29] (the heavy quark-antiquark free energy was defined by McLerran and Svetitsky in [30]) and also studied in lattice QCD (see, e.g., [31–33] for reviews). We recall that the free energy describes a thermodynamical property of the system and it is computed from the static quark-antiquark propagator evaluated at the imaginary time $1/T$ (for large temperatures this corresponds to small imaginary times), while the static energy studied in this work describes the real-time evolution of a quark-antiquark pair and it is computed by

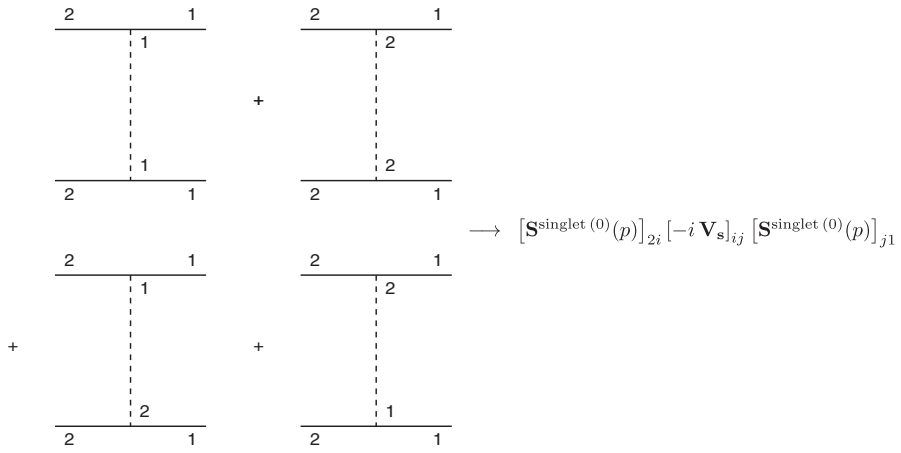

FIG. 15. Matching condition for $[-i\mathbf{V_s}]_{21}$.

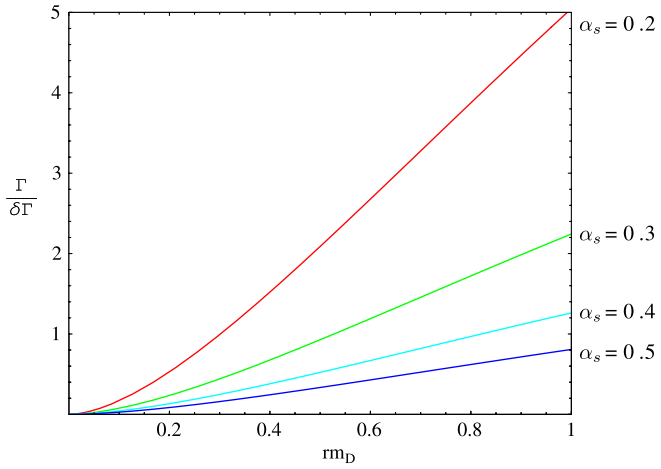

FIG. 16 (color online). $\Gamma/\delta\Gamma$ vs rm_D for different values of α_s.

evaluating the quark-antiquark propagator at infinite real times. The thermal decay width (113) coincides with the result of Ref. [5].

E. The $1/r \gg m_D$ case

In the $1/r \gg m_D$ case, but with m_D still larger than the binding energy, the scales $1/r$ and m_D are integrated out in two subsequent matchings. First, the matching at the scale $1/r$ can be done in close analogy with the discussion in Secs. VI A, VI B, and VI C. The potential is given by Eqs. (107)–(110): since $|\vec{k}| \sim 1/r \gg m_D$ we expand $\mathbf{D}_{00}(0,\vec{k})$ in powers of $m_D^2/\vec{k}^2$. We need to regularize the integrals because after expansion they become infrared divergent:

$$\begin{aligned} V_s(r) &= \mu^{4-d}\int \frac{d^{d-1}k}{(2\pi)^{d-1}} e^{-i\vec{k}\cdot\vec{r}} \\ &\quad\times\left[-C_F\frac{4\pi\alpha_s}{\vec{k}^2}\left(1-\frac{m_D^2}{\vec{k}^2}+\cdots\right)\right. \\ &\quad\left.+\,iC_F\frac{T}{|\vec{k}|}m_D^2\frac{4\pi^2\alpha_s}{\vec{k}^4}(1+\cdots)\right] \\ &= -C_F\frac{\alpha_s}{r}-\frac{C_F}{2}\alpha_s r m_D^2+\cdots+i\frac{C_F}{6}\alpha_s r^2 T m_D^2 \\ &\quad\times\left(\frac{1}{\epsilon}+\gamma_E+\ln\pi+\ln(r\mu)^2-1\right)+\cdots. \end{aligned} \tag{114}$$

The dots stand for higher-order real and imaginary terms. In the Coulomb part, we have displayed only the leading term. In the imaginary part, the divergence comes from the Fourier transform of $1/|\vec{k}|^5$, which, in d dimensions, may be found in [34]. Because we expand the gluon propagator in $m_D^2/\vec{k}^2$ the integral corresponding to the static quark self-energy has no scale and the matching gives $\delta m = 0$.

Next, we integrate out the scale m_D. At one-loop level this corresponds to evaluating the contribution to the potential of the diagram generated by the singlet-octet vertex (dipole interaction) in the effective theory, which is shown in Fig. 5; the HTL resummed gluon propagator is used. Therefore, the contribution is the same as the one calculated in Sec. IV D 2 and given in Eq. (87). Summing its diagonal element with Eq. (114) gives

$$\begin{aligned} V_s(r) &= -C_F\frac{\alpha_s}{r}-\frac{C_F}{2}\alpha_s r m_D^2+\frac{C_F}{6}\alpha_s r^2 m_D^3+\cdots \\ &\quad -i\frac{C_F}{6}\alpha_s r^2 T m_D^2\left(-2\gamma_E-\ln(rm_D)^2+\frac{8}{3}\right)+\cdots. \end{aligned} \tag{115}$$

We see that in the sum the divergences of Eqs. (87) and (114) cancel each other providing a finite physical result. The term $\frac{C_F}{6}\alpha_s r^2 m_D^3$ in the real part is suppressed by a factor rm_D with respect to $-\frac{C_F}{2}\alpha_s r m_D^2$ and will be neglected in the following. Note the appearance of the logarithm $\ln(rm_D)^2$ opposed to the appearance of the logarithm $\ln\frac{T^2}{m_D^2}$ in Eq. (92). In the first case, the logarithm signals that divergences have been canceled when integrating out the scales $1/r$ and m_D;, in the second case it signals that divergences have been canceled when integrating out the scales T and m_D. The real and imaginary parts of Eq. (115) can be also obtained by expansion in rm_D of Eq. (112) and $-\Gamma/2$, as defined in Eq. (113), respectively.

F. Singlet static energy for $1/r \gg m_D$

The real part of Eq. (115) provides the static quark-antiquark energy for $1/r \gg m_D$, whose leading thermal contribution is

$$\delta E_s = -\frac{C_F}{2}\alpha_s r m_D^2, \tag{116}$$

and minus twice the imaginary part of Eq. (115) provides the static quark-antiquark thermal decay width

$$\Gamma = \frac{C_F}{3}\alpha_s r^2 T m_D^2\left(-2\gamma_E-\ln(rm_D)^2+\frac{8}{3}\right). \tag{117}$$

Also in this case the singlet to octet breakup process provides a contribution to the thermal width, which is $\delta\Gamma = \frac{1}{3}N_c^2 C_F\alpha_s^3 T$. This contribution is parametrically suppressed by a factor $(\Delta V/m_D)^2$ with respect to the one in (117). However, depending on α_s and rm_D, it may still contribute to a large fraction of Γ; see Fig. 16. Note that the condition $m_D \gg \Delta V$ requires $\alpha_s(1/r) \ll 2/N_c \times rm_D$ to be fulfilled.

VII. CONCLUSIONS

We have studied the real-time evolution of a static quark-antiquark pair in a medium of gluons and light quarks characterized by a temperature T. We have addressed the problem of defining and deriving the potential between the two static sources, and of calculating their

energy and thermal decay width. In the different ranges of temperature considered, we have set up and worked out a suitable sequence of effective field theories. Our framework has been very close to the modern EFT treatment of nonrelativistic and static bound states at zero temperature [10], but complicated by the existence of the thermal scales T and m_D. We have assumed that all the energy scales are perturbative and worked in a strict weak-coupling framework. This had two consequences: first, we could exploit the hierarchy $T \gg m_D$, and second, the potential that we obtained is valid in the short range. In an EFT framework, the potential is the r-dependent matching coefficient that appears in front of the four-fermion operator that destroys and creates the bound state, after having integrated out all scales above the bound-state energy. Higher-order operators give lower energy contributions, entering into the computation of physical observables, but not in the Schrödinger equation that governs the motion of the bound state and hence are not of a potential type.

A systematic treatment of nonrelativistic bound states in a thermal medium, in an EFT framework and in real-time formalism, has to our knowledge not been presented so far. We have devoted several parts of this work to set up a proper real-time formalism for static sources. The main outcome of this more formal aspect of the paper is in Eq. (60), which expresses the real-time quark-antiquark propagator as an infinite sum of free propagators and potential or mass-shift insertions. In all the considered dynamical regimes, the structure of the potential is such to satisfy this equation; see Eqs. (58), (91), (100), and (101).

We have considered a wide range of temperatures and provided the leading thermal effects to the potential. The results may be summarized in the following way. (1) If the temperature is smaller than or as large as the bound-state energy scale, there are no thermal contributions to the potential, which is simply the Coulomb potential (58). Thermal effects enter in physical observables in loop corrections induced by low-energy gluons. The static energy and the thermal width of the system have been calculated in (88) and (89). The system exhibits a thermal width, because, due to thermal fluctuations, at short range a color-singlet quark-antiquark state may break up into an octet state and gluons. This is a novel feature of quark-antiquark bound states in a thermal medium that, to our knowledge, has not been considered quantitatively before. The singlet to octet breakup mechanism provides the dominant contribution to the thermal width when the temperature is as large as the bound-state energy. (2) If the temperature is larger than the bound-state energy scale but smaller than $1/r$ and if m_D is smaller than or as large as the bound-state energy scale, then the leading thermal correction to the Coulomb potential is given by the sum of Eqs. (73) and (82). The potential develops a real and an imaginary part. Both the singlet to octet thermal breakup mechanism and the imaginary part of the gluon self-energy induced by the Landau damping phenomenon contribute to the imaginary part. If m_D is smaller than the bound-state energy scale then the singlet to octet thermal breakup provides parametrically the dominant contribution to the decay width. The imaginary part of the potential originated by the imaginary part of the gluon self-energy is divergent and needs to be regularized. In physical observables, the divergent part cancels against contributions coming from the scale m_D. (3) If also m_D is larger than the bound-state energy scale, then a diagram similar to Fig. 5 with HTL resummed gluon propagators contributes to the potential as well. The expression of the potential turns out to be finite at the considered order and is given by Eq. (92). Equation (92) is finite because it provides the leading thermal correction to the static energy and to the decay width in the expansions in $\Delta V/T$, m_D/T, and rm_D. The same result has been also derived in perturbative QCD by calculating the Fourier transform of the diagrams in Figs. 9 and 11. (4) If the temperature is larger than $1/r$ but m_D is smaller than $1/r$, the static potential is given by Eq. (115). If m_D is also smaller than or of the same order as ΔV then the potential is given by Eq. (114) and divergences cancel in physical observables against loop corrections from the scale m_D. (5) Finally, if m_D is of the order of $1/r$ the static potential is given by Eq. (111): this result agrees with the earlier finding of [5]. Equations (111) and (115) are finite because, in the kinematical regions of validity, they provide the leading thermal correction to the static energy and the decay width [see Eqs. (112), (113), (116), and (117)]. In the temperature ranges (3), (4), and (5), the parametrically dominant contribution to the thermal width comes from the imaginary part of the gluon self-energy.

While this work was being carried out and completed some papers appeared dealing with some of the issues addressed here. In [35,36], among others, the role of the gluon condensate was considered. The gluon condensate enters the expression of the mass of the quarkonium if the typical binding energy is much larger than the hadronic scale $\Lambda_{\rm QCD}$. The potential is therefore not affected, while the effect of the gluon condensate on the mass is parametrically smaller than the leading relativistic corrections. If the temperature scale is larger than the binding energy then the temperature enters the potential and the effects have been described in the present work. If $T \ll 1/r$, temperature effects are carried by the dipole-dipole interaction shown in Fig. 5 and corrections to it. Only when the time scale of the chromoelectric correlator is smaller than the binding-energy scale, the chromoelectric correlator reduces to the local condensate (see Sec. IV C). Low temperatures, smaller than the binding energy, affect the condensate but not the potential, which remains Coulombic. In this case, thermal effects [in the static limit, they have been evaluated in Eq. (90)] are parametrically smaller than the leading relativistic corrections. It remains

to be clarified if a temperature scale below the binding energy is above the critical temperature: this may depend on the fact that the temperature scale is T or a multiple of πT. In [37], some of the issues discussed here about the potential in real-time formalism have been addressed. In particular, static particles in real-time formalism have been considered and Eq. (111) has been derived for a hot QED plasma in a real-time framework. It has been also pointed out that the real part of the static potential (111) agrees with the singlet free energy and that for large separations $r \gg 1/m_D$, $\Gamma/2$, as defined in Eq. (113), gives twice the damping rate of an infinitely heavy quark. Finally, in [38] a study of nonrelativistic bound states in a hot QED plasma has been carried out in a nonrelativistic EFT framework, which is similar to the one presented here.

There are many possible developments of this work, some of which have already been mentioned in the previous pages. Here we stress a few of them. First, the construction of a full EFT for nonrelativistic bound states at finite temperature requires to be completed. We have focused in the paper on the quark-antiquark color-singlet state, but a complete identification and study of all relevant degrees of freedom that appear once the thermal energy scales have been integrated out, is still to be done. This may require the construction of an EFT that includes the dynamics of gauge fields below the scale m_D [39]. Second, in the EFT framework presented here, the study of quark-antiquark states at large but finite mass, i.e., actual quarkonium in a thermal medium, should be addressed. As argued in the paper, the static limit provides the first piece of a $1/m$ expansion; higher-order corrections may be systematically implemented in the framework of NRQCD and pNRQCD. Finally, although the short-distance analysis performed in this work may provide a valuable tool for studying the thermal dissociation of the lowest quarkonium resonances, the inclusion in the analysis of the nonperturbative scale $\Lambda_{\rm QCD}$ may become necessary for studying excited states. Also in this case, it should be investigated first what are the relevant degrees of freedom in a thermal medium once $\Lambda_{\rm QCD}$ has been integrated out and, in particular, the fate of the color-octet quark-antiquark state (see also [40]).

ACKNOWLEDGMENTS

N. B. and A. V. would like to thank the Instituto de Física Corpuscular (IFIC) of Valencia for the warm hospitality and the stimulating atmosphere provided when a large part of this work was being carried out. N. B. and A. V. thank Miguel Escobedo Espinosa and Joan Soto for discussions, for reading the manuscript, and for sharing their results with us before publication. A. V. acknowledges financial support by the IFIC. N. B. and A. V. acknowledge financial support from the network Flavianet (EU) No. MRTN-CT-2006-035482. The work of P. P. has been supported by the U.S. Department of Energy under Contract No. DE-AC02-98CH10886.

[1] T. Matsui and H. Satz, Phys. Lett. B **178**, 416 (1986).
[2] F. Karsch, M. T. Mehr, and H. Satz, Z. Phys. C **37**, 617 (1988).
[3] S. Digal, P. Petreczky, and H. Satz, Phys. Lett. B **514**, 57 (2001); Phys. Rev. D **64**, 094015 (2001).
[4] Á. Mócsy and P. Petreczky, Phys. Rev. D **73**, 074007 (2006); Phys. Rev. Lett. **99**, 211602 (2007); Phys. Rev. D **77**, 014501 (2008).
[5] M. Laine, O. Philipsen, P. Romatschke, and M. Tassler, J. High Energy Phys. 03 (2007) 054.
[6] M. Laine, J. High Energy Phys. 05 (2007) 028.
[7] M. Laine, O. Philipsen, and M. Tassler, J. High Energy Phys. 09 (2007) 066.
[8] A. Jakovac, P. Petreczky, K. Petrov, and A. Velytsky, Phys. Rev. D **75**, 014506 (2007).
[9] M. Le Bellac, *Thermal Field Theory* (Cambridge University Press, Cambridge, England, 1996), p. 256.
[10] N. Brambilla, A. Pineda, J. Soto, and A. Vairo, Rev. Mod. Phys. **77**, 1423 (2005).
[11] W. E. Caswell and G. P. Lepage, Phys. Lett. **167B**, 437 (1986); G. T. Bodwin, E. Braaten, and G. P. Lepage, Phys. Rev. D **51**, 1125 (1995); **55**, 5853(E) (1997).
[12] P. V. Landshoff and A. Rebhan, Nucl. Phys. **B383**, 607 (1992); **B406**, 517(E) (1993).
[13] E. Braaten and R. D. Pisarski, Nucl. Phys. **B337**, 569 (1990); **B339**, 310 (1990); J. Frenkel and J. C. Taylor, Nucl. Phys. **B334**, 199 (1990).
[14] J. Ghiglieri, Master's Thesis, Università degli Studi di Milano, 2008..
[15] J. I. Kapusta and C. Gale, *Finite-Temperature Field Theory: Principles and Applications* (Cambridge University Press, Cambridge, England, 2006), p. 428.
[16] U. W. Heinz, K. Kajantie, and T. Toimela, Ann. Phys. (N.Y.) **176**, 218 (1987); K. Kajantie and J. I. Kapusta, Ann. Phys. (N.Y.) **160**, 477 (1985).
[17] M. E. Carrington, Hou Defu, and M. H. Thoma, Eur. Phys. J. C **7**, 347 (1999).
[18] A. Pineda and J. Soto, Nucl. Phys. B, Proc. Suppl. **64**, 428 (1998).
[19] N. Brambilla, A. Pineda, J. Soto, and A. Vairo, Nucl. Phys. **B566**, 275 (2000).
[20] N. Brambilla, A. Pineda, J. Soto, and A. Vairo, Phys. Rev. D **60**, 091502 (1999).
[21] A. Schäfer and M. H. Thoma, Phys. Lett. B **451**, 195 (1999).
[22] E. Braaten and R. D. Pisarski, Phys. Rev. D **45**, R1827

(1992).
[23] D. Kharzeev and H. Satz, Phys. Lett. B **334**, 155 (1994).
[24] N. Brambilla, X. Garcia i Tormo, J. Soto, and A. Vairo, Phys. Lett. B **647**, 185 (2007).
[25] C. A. Flory, Phys. Lett. **113B**, 263 (1982); R. A. Bertlmann and J. S. Bell, Nucl. Phys. **B227**, 435 (1983).
[26] E. Gava and R. Jengo, Phys. Lett. **105B**, 285 (1981).
[27] P. Petreczky, Eur. Phys. J. C **43**, 51 (2005).
[28] R. D. Pisarski, Phys. Rev. D **47**, 5589 (1993).
[29] S. Nadkarni, Phys. Rev. D **34**, 3904 (1986).
[30] L. D. McLerran and B. Svetitsky, Phys. Rev. D **24**, 450 (1981).
[31] O. Kaczmarek, F. Karsch, P. Petreczky, and F. Zantow, Phys. Lett. B **543**, 41 (2002).
[32] O. Kaczmarek, F. Karsch, F. Zantow, and P. Petreczky, Phys. Rev. D **70**, 074505 (2004); **72**, 059903(E) (2005).
[33] N. Brambilla *et al.* (Quarkonium Working Group), CERN Report No. CERN-2005-005, 2005.
[34] I. M. Gelfand, *Generalized Functions* (Academic Press, New York, 1964), p. 423.
[35] D. E. Kharzeev, J. Phys. G **34**, S445 (2007).
[36] S. H. Lee and K. Morita, arXiv:0802.4000.
[37] A. Beraudo, J. P. Blaizot, and C. Ratti, arXiv:0712.4394.
[38] M. Escobedo and J. Soto, Report No. UB-ECM-PF 08/05.
[39] D. Bödeker, Phys. Lett. B **426**, 351 (1998).
[40] O. Jahn and O. Philipsen, Phys. Rev. D **70**, 074504 (2004).